BRAIN

ORIGINAL ARTICLE

Targeted blockade of aberrant sodium current in a stem cell-derived neuron model of SCN3A encephalopathy

Guojie Qu,[1,†] Julie P. Merchant,[2,†] Jérôme Clatot,[1,3,†] Leah M. DeFlitch,[1] Danny J. Frederick,[4] Sheng Tang,[2] Madeleine Salvatore,[4] Xiaohong Zhang,[1] Jianping Li,[4,‡] Stewart A. Anderson[3,4,5] and Ethan M. Goldberg[1,2,3,6]

†These authors contributed equally to this work.

Missense variants in *SCN3A* encoding the voltage-gated sodium (Na⁺) channel α subunit Na$_v$1.3 are associated with *SCN3A*-related neurodevelopmental disorder (SCN3A-NDD), a spectrum of disease that includes epilepsy and malformation of cortical development. How genetic variation in *SCN3A* leads to pathology remains unclear, as prior electrophysiological work on disease-associated variants has been performed exclusively in heterologous cell systems. To further investigate the mechanisms of SCN3A-NDD pathogenesis, we used CRISPR/Cas9 gene editing to modify a control human induced pluripotent stem cell (iPSC) line to express the recurrent *de novo* missense variant *SCN3A* c.2624T>C (p.Ile875Thr).

With the established Ngn2 rapid induction protocol, we generated glutamatergic forebrain-like neurons (iNeurons), which we showed to express *SCN3A* mRNA and Na$_v$1.3-mediated Na⁺ currents. We performed detailed whole-cell patch clamp recordings to determine the effect of the *SCN3A*-p.Ile875Thr variant on endogenous Na⁺ currents in, and intrinsic excitability of, human neurons. Compared to control iNeurons, variant-expressing iNeurons exhibit markedly increased slowly-inactivating/persistent Na⁺ current, abnormal firing patterns with paroxysmal bursting and plateau-like potentials with action potential failure, and a hyperpolarized voltage threshold for action potential generation. We then validated these findings using a separate iPSC line generated from a patient harbouring the *SCN3A*-p.Ile875Thr variant compared to a corresponding CRISPR-corrected isogenic control line. Finally, we found that application of the Na$_v$1.3-selective blocker ICA-121431 normalizes action potential threshold and aberrant firing patterns in *SCN3A*-p.Ile1875Thr iNeurons; in contrast, consistent with action as a Na⁺ channel blocker, ICA-121431 decreases excitability of control iNeurons.

Our findings demonstrate that iNeurons can model the effects of genetic variation in *SCN3A* yet reveal a complex relationship between gain-of-function at the level of the ion channel versus impact on neuronal excitability. Given the transient expression of *SCN3A* in the developing human nervous system, selective blockade or suppression of Na$_v$1.3-containing Na⁺ channels could represent a therapeutic approach towards SCN3A-NDD.

1 Division of Neurology, Department of Pediatrics, The Children's Hospital of Philadelphia, Philadelphia, PA, 19104, USA
2 Department of Neuroscience, University of Pennsylvania Perelman School of Medicine, Philadelphia, PA, 19104, USA
3 The Epilepsy NeuroGenetics Initiative, The Children's Hospital of Philadelphia, Philadelphia, PA, 19104, USA
4 Department of Child and Adolescent Psychiatry, The Children's Hospital of Philadelphia, Philadelphia, PA, 19104, USA
5 Department of Psychiatry, University of Pennsylvania Perelman School of Medicine, Philadelphia, PA, 19104, USA
6 Department of Neurology, University of Pennsylvania Perelman School of Medicine, Philadelphia, PA, 19104, USA

‡ Present address: Department of Psychiatry, First Affiliated Hospital, Zhejiang University School of Medicine, Hangzhou, China

Correspondence to: Ethan M. Goldberg, MD, PhD
The Children's Hospital of Philadelphia, Abramson Research Center Room 510D, 3615 Civic Center Boulevard
Philadelphia, PA, 19104, USA
E-mail: goldberge@chop.edu

Correspondence may also be addressed to: Stewart A. Anderson, MD
The Children's Hospital of Philadelphia, Abramson Research Center
Room 517, 3615 Civic Center Boulevard
Philadelphia, PA, 19104, USA
E-mail: sande@pennmedicine.upenn.edu

Introduction

Sodium (Na$^+$) channels are critical regulators of neuronal excitability via the generation and propagation of action potentials (APs). Genetic variants in brain-expressed Na$^+$ channel genes *SCN1A*, *SCN2A*, *SCN3A*, *SCN8A* and *SCN1B* (encoding the pore-forming α subunits Na$_v$1.1, 1.2, 1.3 and 1.6, and the β-subunit Na$_v$β2, respectively) are established causes of epilepsy.[1-5] Variants in *SCN3A* cause *SCN3A*-related neurodevelopmental disorder (SCN3A-NDD), a spectrum of neurological dysfunction that includes developmental delay and intellectual disability (ID), speech/language impairment, epilepsy of varying severity and, surprisingly, malformation of cortical development (MCD). *De novo* heterozygous missense variants in *SCN3A* generally produce a syndrome of severe-to-profound global developmental delay and functional impairment, early-onset treatment-resistant epilepsy and, in many but not all cases, MCD characterized as multifocal or diffuse dysgyria.[1,6-9] Understanding the mechanistic basis of how genetic variation in *SCN3A* leads to neurological disease could inform the development of novel therapeutic approaches for SCN3A-NDD, which is currently an untreatable condition associated with high morbidity and childhood mortality.

We recently reported detailed clinical, genetic and neuroimaging data on a cohort of over 20 patients with SCN3A-NDD as well as the electrophysiological properties of Na$^+$ channels containing the identified patient-specific Na$_v$1.3 variants via voltage clamp recording in a heterologous system.[2] We found that disease-associated variants exhibited so-called gain of ion channel function, with a left/hyperpolarized shift in the voltage dependence of activation and/or increased slowly inactivating/persistent current. Recently, neurons generated from induced pluripotent stem cells (iPSCs) derived from human patients have been used to advance beyond heterologous systems to model the impact of epilepsy-associated variants on neuronal function, including for Na$^+$ channelopathies such as Dravet syndrome[10,11] and *SCN8A* encephalopathy,[12] epilepsy-associated potassium channelopathies[13] and other causes of epileptic encephalopathy.[14,15]

SCN3A encodes the voltage-gated Na$^+$ channel pore-forming (α) subunit Na$_v$1.3, which is expressed throughout the nervous system at early developmental time points in humans and rodents,[16-20] including expression in radial glial cells, intermediate progenitors and developing neurons of the embryonic brain.[6] Hence, given the immature/developing state of neurons generated using standard induction protocols,[21-23] the iPSC-derived neuron system is well positioned to model the impact of pathogenic variants in *SCN3A* on the function of developing neurons.

Here, using CRISPR/Cas9 gene editing in a control human iPSC line, we generated a modified line harbouring the most common recurrent *de novo* variant SCN3A c.2624T>C (p.Ile875Thr), identified in at least 10 patients reported in the literature.[1,2,8] With the rapid neurogenin-2 (Ngn2) induction protocol,[24] we differentiate iPSCs into developing forebrain-like glutamatergic neurons (iNeurons) and confirm that iNeurons express *SCN3A* transcripts and functional Na$_v$1.3-containing Na$^+$ channels, mirroring what is seen in early human brain development. We performed whole-cell voltage clamp recording of Na$^+$ currents in cultured iNeurons at each of three differentiation time windows and find that *SCN3A*-p.Ile875Thr variant-expressing iNeurons exhibit increased slowly-inactivating/persistent current relative to control, consistent with prior results in heterologous systems. We then performed current clamp recording in iNeurons during the same differentiation time windows to assess intrinsic excitability and AP generation. While variant-expressing iNeurons show a lower (hyperpolarized) voltage threshold for AP generation and paroxysmal bursting behaviour suggesting hyperexcitability, a subset of iNeurons exhibit an overall lower maximal evoked firing rate likely due to acceleration of depolarization block. We then validated these results in iNeurons using a separate iPSC line derived from a human patient harbouring the same pathogenic variant (*SCN3A*-p.Ile875Thr) and a CRISPR/Cas9-corrected isogenic control line. Finally, we implemented Na$_v$1.3-specific pharmacology using the Na$_v$1.3-selective antagonist ICA-121431.[25] Low concentrations of ICA-121431 lead to depolarization of AP threshold, block of paroxysmal firing, and a seemingly paradoxical increase in firing frequency in *SCN3A*-p.Ile875Thr iNeurons exhibiting bursting/plateau. Our results suggest complex effects of a recurrent epilepsy-associated *SCN3A* variant on neuronal excitability and the possibility that Na$_v$1.3-selective blockers could represent a therapeutic approach towards treatment of SCN3A-NDD, particularly given the developmentally delimited expression of Na$_v$1.3-containing Na$^+$ channels in the human brain.

Materials and methods

Induced pluripotent stem cell line generation

A male iPSC control line ND1.4 (RRID: CVCL_1E77) was obtained from the NINDS Human Cell and Data Repository. This line was subcloned and confirmed to be karyotypically normal and without detectable copy number variants (CNVs) (Supplementary Fig. 1A and B). The subclone was then modified using CRISPR/Cas9 gene editing as previously described[26,27] to specifically introduce the

SCN3A c.2624T>C missense variant on one allele resulting in a p.Ile875Thr amino acid substitution (based on NCBI RefSeq NM_006922.4 and NCBI RefSeq NP_008853.3 for human SCN3A isoform 1). Following cloning of single-cell derived colonies, correct editing was confirmed in one clone via Sanger sequencing and CNV analysis (Supplementary Fig. 1B and C).

Separately, a blood sample was obtained from a male patient harbouring the SCN3A c.2624T>C, p.Ile875Thr variant (Patient 1 from our previous publication[1]) after informed consent was provided by parents/legal guardians according to the Declaration of Helsinki (as the patient was a minor with intellectual disability), under a protocol approved by the Institutional Review Board at The Children's Hospital of Philadelphia. At the time the sample was obtained, the patient was a 13-year-old male with chronic static encephalopathy with severe intellectual disability, microcephaly and treatment-resistant epilepsy, with onset at age 2 weeks. Brain MRI revealed malformations of cortical development with diffuse polymicrogyria and frontoparietal predominant cortical thickening. Trio whole exome sequencing identified a heterozygous de novo variant in SCN3A c.2624T>C (p.Ile875Thr). At most recent follow-up, at age 18 years, the patient remained non-verbal and non-ambulatory with feeding via gastrostomy tube. IPSCs were reprogrammed from peripheral blood mononuclear cells according to published protocols.[28] Three single-cell derived clones were expanded and characterized via Sanger sequencing, DNA fingerprinting, karyotyping, Sendai clearance analysis, stem cell marker expression and trilineage differentiation (Supplementary Fig. 1D–J). In one clone of the patient-derived line, the heterozygous SCN3A c.2624T>C variant was corrected using CRISPR/Cas9-mediated gene editing as previously described[26,27] to generate an isogenic control iPSC line. Four correctly edited single-cell derived clones were validated via Sanger sequencing and CNV analysis (Supplementary Fig. 1K and L).

See Supplementary material for further details on cell line reprogramming, validation and quality control assays.

Induced pluripotent stem cell culture and differentiation

One clone of each iPSC line generated in this study was used for all rounds of differentiation of that line (Supplementary material); herein all references to a given line also denote the particular clone utilized. The selected clone for each CRISPR/Cas9-edited line was confirmed to show evidence of biallelic amplification based on the sequencing data (Supplementary Fig. 1C and K), thus ensuring that copy-neutral loss of heterozygosity had not occurred, as recommended by Simkin et al.[29] IPSCs were maintained in StemMACS[TM] iPS-Brew XF human (Miltenyi Biotec) and each line was transduced with two lentiviral vectors—TetO-mNgn2-T2A-PuroR and Ubiq-rtTA, as described previously[30]—to generate doxycycline-inducible Ngn2-infected iPSC lines. See Supplementary material for further details on iPSC culture and lentiviral transduction.

Induced differentiation of human iPSCs to neurons in co-culture with primary rat astrocytes was accomplished by an established protocol[24] with minor modifications, as described previously.[30] Briefly, on Day 0, differentiation was initiated with exposure to doxycycline (2 μg/ml, Sigma-Aldrich) followed by puromycin (5 μg/ml, Sigma-Aldrich) 24 h later to select for cells that had successfully integrated the lentiviral vectors. Cells were replated on Day 2 onto Matrigel-coated 12 mm round glass coverslips in a 24-well plate at 50 000 cells/well. Rat glia, when used, were plated on Day 4 onto neurons at an additional 50 000 cells/well. A single administration of 2 μM Ara-C (Sigma-Aldrich) was added on Day 6. Doxycycline was discontinued on Day 10. From Day 14 onwards, co-culture medium was changed to BrainPhys[TM] Neuronal Medium supplemented with N2-A and SM1 (STEMCELL Technologies). iNeurons were cultured with a half volume media change every 2–3 days until used for further analysis. See Supplementary material for further details on iNeuron differentiation and rat glia preparation.

RT-qPCR

Total RNA was extracted using TRIzol (Ambion, Thermo Fisher Scientific) from three wells per line at Days 7, 17, 28 and 42 of differentiation. RNA concentration was measured using a NanoDrop 2000 spectrophotometer (Thermo Fisher Scientific). cDNA was generated using SuperScript[TM] III First-Strand Synthesis System for RT-PCR (Invitrogen). The presence of the SCN3A-c.2624T>C variant was confirmed in cDNA from differentiation day (DD)7 variant samples and its absence in DD7 control samples by PCR and gel electrophoresis using custom-designed primers, as well as by Sanger sequencing of the PCR product. Gene expression was measured by RT-qPCR on a Fisher QuantStudio 3 Real-time PCR machine using TaqMan[TM] Universal PCR Master Mix (Applied Biosystems, Thermo Fisher Scientific) for human SCN1A (Hs00374696_m1), SCN2A (Hs00221379_m1), SCN3A (Hs00366902_m1), SCN8A (Hs00274 075_m1) and ACTB (Hs99999903_m1), with each sample run in triplicate per gene. All primer pairs were purchased from Thermo Fisher Scientific. Data were analysed using the ΔCt method, where ΔCt (threshold cycle) = mean Ct of target gene − mean Ct of the housekeeping gene β-actin, and presented as relative expression ($2^{-\Delta Ct} \times 100$) in order to compare developmental changes in relative Na^+ channel gene expression across the four time points of differentiation.

Immunocytochemistry

iNeurons on coverslips were fixed with 4% paraformaldehyde (PFA) for 10 min, followed by membrane permeabilization and blocking with 0.1% Triton X-100 and 10% normal goat serum in 1× PBS. Immunostaining was performed for MAP2 (1:500; Sigma-Aldrich M4403) and TUJ1 (1:500; Abcam ab18207) with the respective secondary antibodies Goat Anti-Mouse Alexa Fluor 488 (Molecular Probes A11029) and Goat Anti-Rabbit Alexa Fluor 568 (Molecular Probes A11036), along with DAPI (1:5000; Molecular Probes D3571). Coverslips were mounted with ProLong[TM] Gold Antifade Mountant on glass slides and allowed to dry prior to imaging. Images were acquired using a Leica THUNDER Imaging System (THUNDER Imager Live Cell and 3D Assay) equipped with Leica Application Suite X (LAS X) software.

Voltage clamp electrophysiology in iNeurons

iNeurons on glass coverslips were individually transferred to a 35 mm dish containing fresh pre-warmed (37°C) BrainPhys[TM] Neuronal Medium (STEMCELL Technologies) and placed on the stage of an inverted epifluorescence microscope (Nikon Ti2) at room temperature (23 ± 1°C) for recording. Intracellular pipette-filling solution contained, in mM: 130 Cs-MetSO$_4$, 6.3 CsCl, 4 Mg-ATP, 0.3 Na$_2$-GTP, 1 MgCl$_2$, 0.5 EGTA, 10 HEPES; pH was adjusted to 7.3 with CsOH, and osmolarity was adjusted to 305 mOsm/l with 30% sucrose, as needed. All chemicals were produced by Sigma-Aldrich. A single coverslip was not used for longer than 2 h.

Recording pipettes were fashioned from thin-walled borosilicate glass (Harvard Apparatus) and fire-polished using a DMZ-Zeitz puller to a resistance of 1.2–2.5 MΩ when placed in extracellular solution. Whole-cell voltage clamp recordings were performed using an Axopatch 200B amplifier coupled to an Axon Digidata 1550B (Molecular Devices). Recordings were initiated when peak current had stabilized (~2 min). Voltage errors were reduced via partial series resistance compensation (50%–80%). Voltage clamp pulses were generated using Clampex 11.2 (Molecular Devices); currents were sampled at 33.3 kHz and filtered at 5 kHz (−3 dB, eight-pole low-pass Bessel filter).

Sodium currents (I_{Na}) were elicited by a repetitive 600 ms pulse at 0.6 Hz to −10 mV from a holding potential of −90 mV. Current was converted to current density (pA/pF) by normalizing to cell capacitance. Persistent current (I_{NaP}) was isolated and measured using a 300 ms test pulse to −10 mV from a holding potential of −90 mV after subtracting traces recorded with perfusion of 500 nM tetrodotoxin (TTX; Abcam). I_{NaP} was quantified as the magnitude of the TTX-sensitive current at 10 and 50 ms after depolarization (to separate an effect on I_{NaP} from any potential effect on fast inactivation) as a percentage of the total peak transient inward current. Linear leak was subtracted *post hoc*. ICA-121431 (Tocris Bioscience) was used to determine the component of I_{Na} mediated by Na_v1.3-containing Na^+ channels. Heterologously expressed human Na_v1.3 is blocked by ICA-121431 with an IC_{50} of 18 ± 5 nM, although block is voltage- and use-dependent with a preference for the inactivated state of the channel; ICA-121431 has been shown to shift the voltage dependence of steady-state inactivation to the left.[21,26,27] We assessed block of I_{Na} in iNeurons in response to 20 nM and 100 nM ICA-121431 using a modified train of pulses to −10 mV from a holding potential of −70 mV at 2 Hz. ICA-sensitive peak and persistent I_{Na} were measured by successive perfusion of ICA-121431 followed by 500 nM TTX. To record multiple iNeurons per coverslip, pharmacological agents ICA-121431 and/or TTX were rapidly applied and washed out during voltage clamp recording using a microfluidic device for brief local perfusion (BioPen, Fluicell). Full *I*-*V* curves could not be reliably constructed and hence voltage dependence of activation could not be calculated due to space clamp issues in some neurons, particularly in response to steps to more depolarized potentials (at/beyond 0 mV). Neurons in which we observed an escape spike in response to step depolarizations were discarded. We found that time to peak upon voltage step to −10 mV in iNeurons was comparable to that obtained in HEK-293T cells transiently transfected with Na_v1.3 (Supplementary Fig. 2), supporting the conclusion that we have adequate voltage control in iNeurons.

Voltage dependence of steady-state Na^+ channel inactivation was determined using a 500 ms prepulse to various potentials (between −140 mV and +5 mV in 5-mV increments) from a holding potential of −120 mV, followed by a 400 ms test pulse to 0 mV, at 1 Hz. The voltage dependence of steady-state channel availability was fitted to the Boltzmann equation:

$$Y = 1/\{1 + \exp[-(V_m - V_{1/2})/k]\} \qquad (1)$$

where V_m is the membrane potential, $V_{1/2}$ is the potential at half-maximal channel availability, and k is the inverse slope factor.

Kinetics of recovery from Na^+ channel inactivation was measured from a holding potential of −90 mV using a 30 ms prepulse to 0 mV followed by a 30 ms test pulse to 0 mV after a variable time delay (in 1-ms increments). The ratio of I_{Na} elicited by the test pulse relative to the prepulse was quantified and plotted relative to the time delay.

We validated the Na_v1.1-specific activator Hm1a (Alomone Labs) in a heterologous (HEK-293T cell) system. See Supplementary material for culture, transfection and voltage clamp recording of Na_v1.1-mediated Na^+ currents in HEK-293T cells related to Supplementary Fig. 4.

All voltage clamp data were analysed with Clampfit 11 (Molecular Devices) and SigmaPlot 14.0 (Systat Software, Inc., San Jose, CA, USA) software.

Current clamp electrophysiology in iNeurons

iNeurons on glass coverslips were transferred individually in BrainPhys™ Neuronal Medium (STEMCELL Technologies) pre-warmed to 37°C to a recording chamber on the stage of an upright microscope (Olympus) and maintained at room temperature for recording. As mentioned earlier, one or more iNeurons were recorded per coverslip and a single coverslip was not used for longer than 2 h. iNeurons were visualized under infrared differential interference contrast (IR-DIC) and individual iNeurons were targeted for recording. Recording pipettes were fashioned from polished thin-walled borosilicate glass (BF150-86-10, Sutter Instruments) using a P-97 puller (Sutter Instruments) and filled with intracellular solution containing, in mM: 130 K-gluconate; 6.3 KCl; 1 MgCl$_2$; 10 HEPES; 0.5 EGTA; 4 Mg-ATP; 0.3 Na$_2$-GTP; pH was adjusted to 7.35 with KOH, and osmolarity adjusted to 290 mOsm/l with 30% sucrose. All chemicals were produced by Sigma-Aldrich. Pipettes had a resistance of 5–7 MΩ when filled and placed in external solution.

Voltage traces were sampled at 100 kHz with a MultiClamp 700B amplifier, filtered at 3–10 kHz, digitized using a Digidata 1550B and acquired using Clampex 11 software (Molecular Devices). Fast pipette capacitance measured after obtaining a giga-Ω seal was compensated and the bridge was balanced after achieving the whole-cell configuration. Only neurons with a resting membrane potential of −30 mV or less (i.e. more hyperpolarized than −30 mV) and which fired one or more APs (as defined later) were included in the analysis. This set of inclusion criteria was designed to reject very immature or non-neuronal cells while attempting to avoid any potential selection bias based on a genotype effect on maturation. Cells for which access resistance increased by >20% during serial monitoring throughout the recording were discarded. We did not correct for liquid junction potential.

Voltage was recorded in response to a series of 600 ms current injection steps from negative current injection and increasing in 3–5 pA increments, with a 4 s inter-sweep interval. Recordings were performed both from spontaneous resting membrane potential (no direct current injection) as well as with the membrane potential held at −70 mV with direct current offset to normalize across cells with variable resting membrane potentials. ICA-121431 was applied via continuous bath perfusion at 20 nM in BrainPhys™; responses were recorded 5 min after application, with washout recorded after another 5 min of perfusion with BrainPhys™ alone.

Data were analysed using custom scripts written in MATLAB R2022b (Mathworks, Natick, MA, USA). Resting membrane potential (V_m) was calculated from the average membrane potential during a sweep with zero current injection. Using the hyperpolarizing responses to negative current injections from −70 mV, input resistance (R_m) was calculated using $R_m = V/I$ and membrane time constant (τ) was calculated from a single exponential fit. All AP parameters were calculated from the first AP generated at rheobase

(determined as the minimum current injection that elicited one or more APs, defined as events that overshot 0 mV and had an amplitude of at least 40 mV with the resting membrane potential held at −70 mV. AP threshold was calculated as the value at which the derivative of the voltage (dV/dt) first reached 10 mV/ms; if a spike-like event did not achieve a dV/dt of 10 mV/ms, it was not considered an AP. AP peak refers to the absolute maximum voltage value of an individual AP, and AP amplitude was calculated as the difference between AP threshold and peak for a given AP. AP rise time was measured as the time from AP threshold to peak and maximum rise slope as the maximal dV/dt within rise time. AP half-width was defined as the width of the AP (in ms) at half-maximal amplitude and APD_{90} as the width of the AP at 90% AP repolarization. AP afterhyperpolarization (AHP) was calculated as the depth of the afterhyperpolarization (in mV) relative to AP threshold.

Maximal steady-state firing frequency was defined as the maximal mean firing frequency during a suprathreshold 600 ms current injection, with a spike defined as an event that overshot 0 mV and had an amplitude of at least 40 mV, as defined earlier. Maximal instantaneous firing frequency was calculated using the smallest interspike interval (ISI) elicited at maximal steady-state firing frequency. Spike frequency adaptation (SFA) was calculated as the ratio of the second to the first ISI (ISI_2/ISI_1) at maximal steady-state firing frequency. Standard f-I curves were constructed using the steady-state firing frequency calculated for each current step, counting failures as 0 for subsequent current steps.

Statistical analysis

Data for standard electrophysiological parameters in iNeurons were typically obtained from at least $n = 10$ cells from at least three coverslips per group, from at least $n = 2$ separate differentiations for each experiment. A total of 16 differentiations (13 of control versus variant lines; three of corrected versus patient) were performed in this study. Exact n of cells recorded per line and time point are reported in each figure legend.

Statistics were generated and plotted using GraphPad Prism 9.0 (GraphPad Software, San Diego, CA, USA), MATLAB R2022b, SigmaPlot 14.0, and Origin (OriginLab Corporation, Northampton, MA, USA). Categorical results (i.e. proportion of firing type grouped by genotype) were assessed by chi-square test. Discrete or continuous results are presented as the mean ± standard deviation (SD) for Na^+ channel gene expression or standard error of the mean (SEM) for all other results. All such data were tested for normality using the Shapiro-Wilk test. Relative Na^+ channel gene expression data ($2^{-\Delta Ct} \times 100$) were analysed via three-way ANOVA, considering genotype, Na^+ channel and day of differentiation as each of three factors, with *post hoc* Bonferroni correction. Electrophysiological data with normal distributions at each time point were compared by two-way ANOVA with *post hoc* Šídák multiple comparisons test when comparing two groups (e.g. genotypes) and with *post hoc* Tukey's multiple comparisons test when comparing three or more groups (e.g. firing types). Electrophysiological data with non-normal distributions at each time point were compared by multiple Wilcoxon rank sum tests with *post hoc* Bonferroni-Dunn's multiple comparisons test (if possible) when comparing two groups, and by Kruskal-Wallis test with *post hoc* Dunn's multiple comparisons test when comparing three or more groups. For pharmacology experiments, those testing the effect of a single concentration of a drug on an electrophysiological parameter were compared by two-tailed paired t-test if the data were normally distributed and by Wilcoxon matched pairs signed rank test if non-normally distributed.

Experiments testing the serial effects of multiple concentrations of ICA-121431 on I_{Na} were analysed using a mixed-effects analysis with *post hoc* Tukey's multiple comparisons test as not all concentrations were tested in every experiment.

Results

iNeurons express SCN3A and functional $Na_v1.3$-containing Na^+ channels

Na^+ channels containing epilepsy-associated variant $Na_v1.3$ subunits largely exhibit 'gain-of-function' alterations in channel activity (GoF; i.e. enhanced Na^+ current), with an increase in the slowly inactivating ('persistent') current component, a leftward/hyperpolarizing shift in the voltage dependence of channel activation, and/or a prolongation in the time constant of fast inactivation.[1,2] However, the impact of such GoF changes on the activity of confirmed $Na_v1.3$-expressing neurons is unknown. To further investigate the mechanisms whereby pathogenic variants in SCN3A might lead to epilepsy, we used CRISPR/Cas9 gene editing to modify a control iPSC line (ND1.4; herein denoted 'Control') to express the recurrent heterozygous variant SCN3A c.2624T>C (p.Ile875Thr) (herein denoted 'Variant'). The p.Ile875Thr variant is the most common recurrent *de novo* variant in SCN3A-NDD ($n = 10$ patients, accounting for 26% of all reported individuals[1,2,8]) and is associated with a severe clinical presentation including neonatal-onset treatment-resistant epilepsy, profound ID and diffuse bilateral polymicrogyria.[9] Using the control versus variant isogenic iPSC line set, we generated iNeurons using a modified version of the rapid Ngn2 induction protocol, which produces developing forebrain-like glutamatergic neurons that are post-mitotic and electrically active by 2 weeks in culture[24] (Fig. 1).

Although SCN3A is known to be highly expressed in the developing nervous system,[16-20] we first confirmed that iNeurons indeed express SCN3A. We performed RT-qPCR for human SCN3A, as well as the other brain-expressed Na^+ channel α subunit transcripts (SCN1A, SCN2A and SCN8A) from both lines at four time points during culture (DD7, 17, 28 and 42). Most notably, we found that SCN3A transcripts are expressed at high levels by DD17 in both control and variant iNeurons (Fig. 1B). SCN2A is also highly expressed in both lines by DD17, whereas SCN1A and SCN8A transcript expression is low at all time points analysed (Fig. 1B), although we did not culture neurons beyond DD41–47. These results demonstrate that our iPSC-derived iNeuron system models the Na^+ channel gene expression pattern seen in early human brain development.[19,20] We additionally note an observed decrease in SCN3A expression at DD42 compared to DD28 (Fig. 1B), suggesting that the iNeuron system in this differentiation time frame may also recapitulate the normal developmental downregulation of SCN3A at later fetal and postnatal stages.[17,31-34]

To confirm that iNeurons exhibit Na^+ currents mediated by $Na_v1.3$ subunit-containing Na^+ channels, we performed whole-cell voltage clamp recordings of Na^+ currents from iNeurons before and after application of the $Na_v1.3$-selective gating inhibitor ICA-121431. Block of $Na_v1.3$-containing Na^+ channels by ICA-121431 is voltage and activity-dependent.[25] As measured in response to a depolarizing pulse to −10 mV from a holding potential of −70 mV, application of 20 nM ICA-121431 blocked 11 ± 2% of peak transient inward Na^+ current in control iNeurons and 23 ± 5% in variant iNeurons and blocked 24 ± 5% of persistent Na^+ current measured 10 ms after depolarization in control iNeurons and 17 ± 7% in variant iNeurons (Fig. 2). ICA-121431 (20 nM and
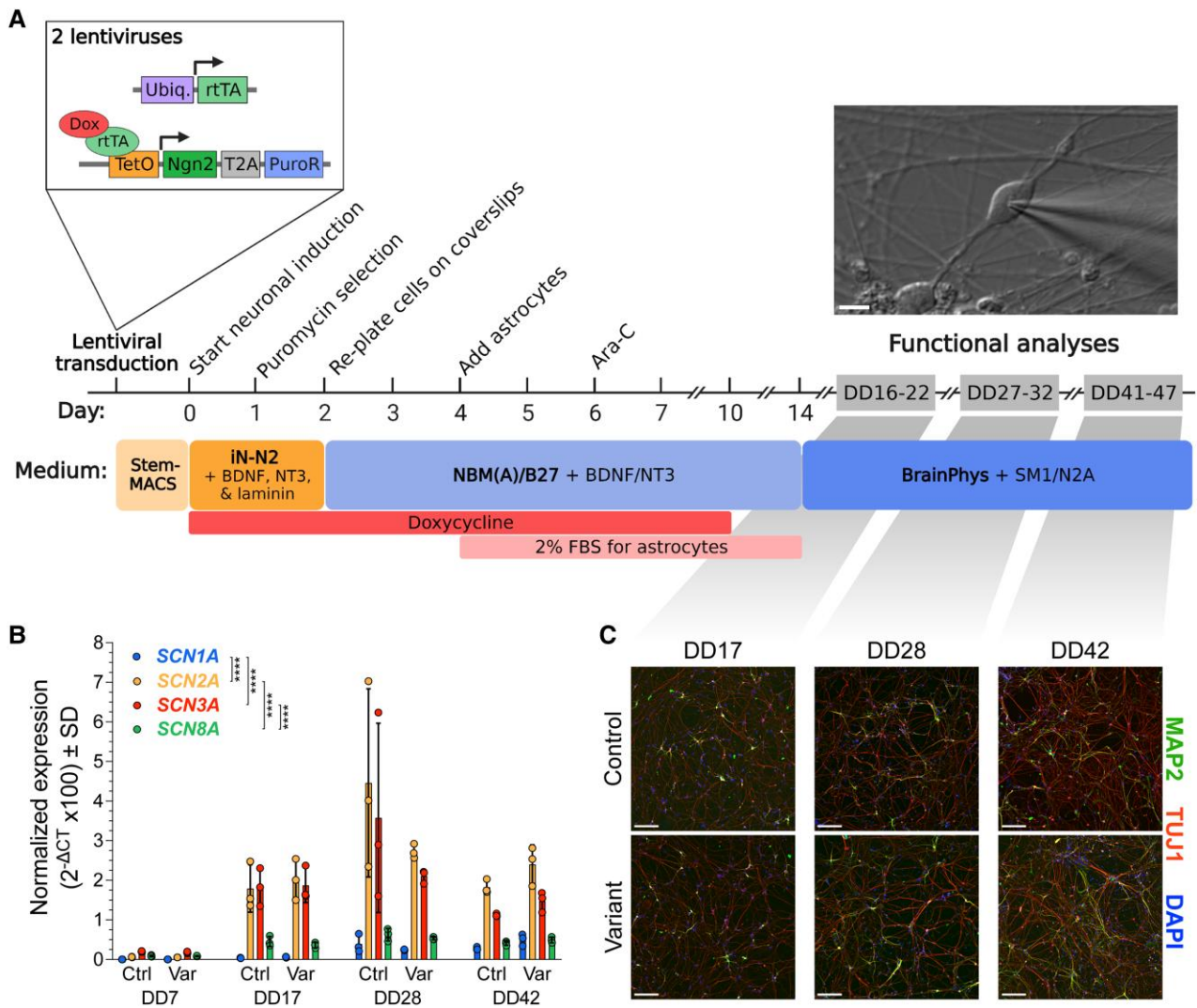
Figure 1 Generation of iPSC-derived neurons (iNeurons) and expression of SCN3A. (**A**) Outline of Ngn2-induced neuron (iNeuron) protocol and experimental timeline. Analysis was performed at three differentiation time windows: DD16–22, 27–32 and 41–47. Shown is a representative infrared differential interference contrast (IR-DIC) image of a control (Ctrl) iNeuron at DD17 during whole-cell patch clamp recording. Scale bar = 10 μm. DD = differentiation day. Created with BioRender.com. (**B**) RT-qPCR of iNeurons confirms high *SCN3A* and *SCN2A* expression and low *SCN1A* and *SCN8A* expression across the differentiation. Relative expression of each Na$^+$ channel gene normalized to the reference gene *ACTB* was quantified from $n = 3$ wells per line per time point; each data-point shown is the average of technical triplicates. Significance was assessed by three-way ANOVA [Genotype $F_{(1,64)} = 0.969$, $P = 0.329$; Na$^+$ channel $F_{(3,64)} = 43.1$, $P < 0.0001$; Time point $F_{(3,64)} = 30.5$, $P < 0.0001$; Genotype × Na$^+$ channel $F_{(3,64)} = 0.332$, $P = 0.802$; Genotype × Time point $F_{(3,64)} = 3.84$, $P = 0.014$; Na$^+$ channel × Time point $F_{(9,64)} = 6.70$, $P < 0.0001$; Genotype × Na$^+$ channel × Time point $F_{(9,64)} = 0.886$, $P = 0.543$]. ****$P < 0.0001$ via *post hoc* test with Bonferroni correction for the Na$^+$ channel factor. (**C**) Immunocytochemistry for MAP2 (green; labels soma and dendrites) and TUJ1 (red; labels neuronal microtubules) demonstrates successful neuronal differentiation with increased neurite outgrowth across days of differentiation, as expected. DAPI (blue) labels nuclei of neurons as well as rat primary astrocytes in co-culture. Scale bar = 200 μm. iPSC = induced pluripotent stem cell; SD = standard deviation; Var = variant.

100 nM) led to a concentration-dependent leftward (hyperpolarized) shift in the voltage dependence of steady-state inactivation in both cell lines (Supplementary Fig. 3), consistent with previous results on the specific effect of ICA-121431 on Na$_v$1.3-containing Na$^+$ channels in heterologous systems[25] and further supporting the conclusion that iNeurons express *SCN3A*. Because ICA-121431 also blocks Na$_v$1.1-containing Na$^+$ channels, albeit with slightly lower potency,[25] we also tested the Na$_v$1.1-specific spider toxin Hm1a, which is an activator of Na$_v$1.1-containing Na$^+$ channels.[35,36] Hm1a (50 nM) had no effect on Na$^+$ currents recorded from iNeurons, yet led to the expected prolongation of Na+ current decay in HEK-293T cells co-transfected with Na$_v$1.1, Na$_v$β1 and Na$_v$β2 (Supplementary Fig. 4). These results, combined with the lack of

detectable SCN1A transcript in iNeurons by RT-qPCR (Fig. 1B), confirm that, between 2.5 and 6 weeks of differentiation, iNeurons express Na$^+$ current mediated in part by Na$_v$1.3 subunit-containing Na$^+$ channels, with little or no expression of Na$_v$1.1.

iNeurons harbouring the epilepsy-associated SCN3A-p.Ile875Thr variant exhibit increased persistent Na$^+$ current

Previous recordings of Na$^+$ channels composed of Na$_v$1.3-p.Ile875Thr variant subunits showed prominent gain of channel function, with a left (hyperpolarized) shift in the voltage dependence of activation and an increase in the slowly-inactivating
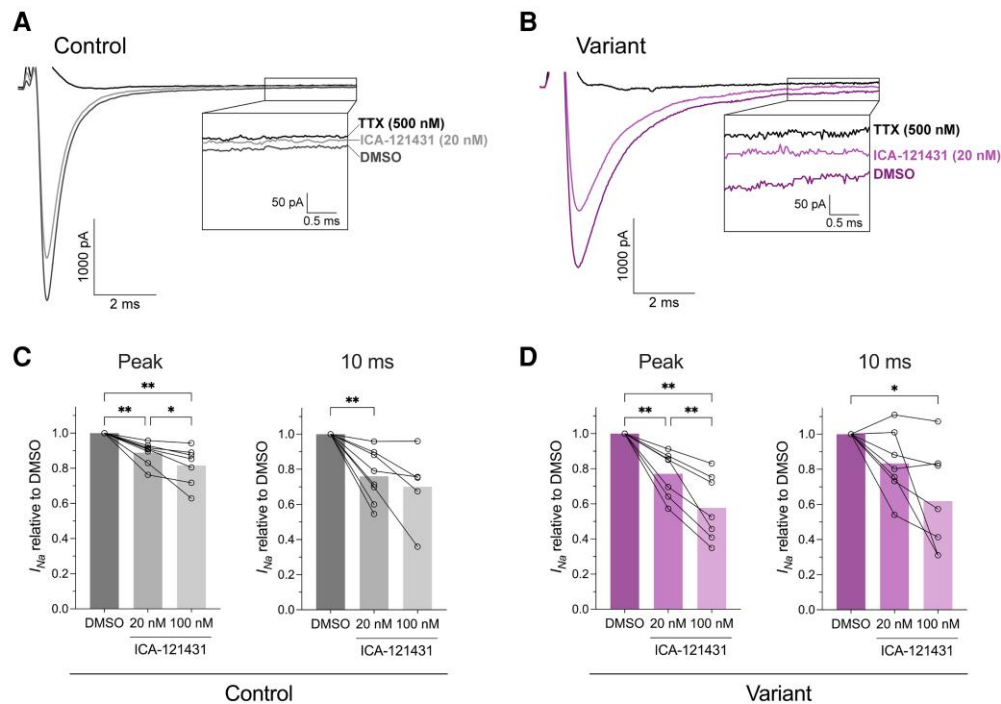
Figure 2 iNeurons express functional Na$^+$ currents sensitive to submicromolar concentrations of the Na$_v$1.3-selective blocker ICA-121431. (A and B) Representative recordings showing inward Na$^+$ currents at differentiation day (DD)17 from control (**A**, dark grey) and variant iNeurons (**B**, purple) in response to depolarization to −10 mV from a −70 mV holding potential in vehicle (dimethyl sulphoxide, DMSO). Lighter traces show remaining Na$^+$ current after perfusion of 20 nM ICA-121431, and black traces show block of all Na$^+$ current after perfusion of 500 nM tetrodotoxin (TTX). Note a larger persistent current component in the variant iNeuron that is partially sensitive to ICA-121431. (**C and D**) Summary data. ICA-121431 at 20 nM and 100 nM blocks similar proportions of peak transient Na$^+$ current and persistent current measured 10 ms after depolarization in control (**C**) and variant (**D**) iNeurons at DD16–22. Shown are values from individual cells, with bars representing mean per condition. Significance was assessed by mixed-effects model (REML) with Geisser-Greenhouse correction (Control-peak $P = 0.0019$, Control-10 ms $P = 0.0028$, Variant-peak $P = 0.0004$, Variant-10 ms $P = 0.011$). *$P < 0.0332$; **$P < 0.0021$; ***$P < 0.0002$; ****$P < 0.0001$; by *post hoc* Tukey's multiple comparisons test. n (control) = 8; n (variant) = 7.

'persistent' current component (I_{NaP}).[1,2] To assess the impact of the *SCN3A*-p.Ile875Thr variant on endogenous Na$^+$ current in iNeurons, we performed whole-cell voltage clamp recordings of Na$^+$ currents from variant versus control lines during three developmental time windows of differentiation (DD16–22, DD27–32 and DD41–47). iNeurons exhibited voltage-dependent transient inward current that was not different in density between genotypes (quantified as pA/pF by normalizing to cell capacitance) at any time point (Supplementary Fig. 5A). Variant iNeurons did, however, show increased I_{NaP} (calculated as a percentage of peak transient inward current) relative to control iNeurons (Fig. 3), consistent with the previously reported effects of this variant in heterologous cells. We observed no differences in voltage dependence of steady-state inactivation (Supplementary Fig. 6A–C) or time course of recovery from inactivation (Supplementary Fig. 7A–C) in variant versus control iNeurons at any time point. Thus, biophysical properties of Na$^+$ currents in *SCN3A*-p.Ile875Thr-expressing iNeurons recapitulate those observed in heterologous systems.

Aberrant firing and hyperexcitability in iNeurons harbouring the epilepsy-associated SCN3A-p.Ile875Thr variant

To assess the electrophysiological impact of the *SCN3A*-p.Ile875Thr variant on neuronal function, we performed whole-cell current clamp recordings of control and variant iNeurons during the same three differentiation time windows. We found that passive membrane properties including resting membrane potential and

input resistance were generally not different between lines (Supplementary Table 1); however, both parameters decreased with duration of time in culture, indicative of neuronal maturation and consistent with what has been observed in studies of similar iPSC-derived neuron models.[22,23,37-39]

As early as DD16, iNeurons from both lines exhibited electro-physiological discharge patterns consistent with immature excitatory cerebral cortex pyramidal cells (Fig. 4A). However, a proportion of neurons exhibited aberrant firing patterns including paroxysmal bursting and plateau-like potentials (Fig. 4A and B and Supplementary Table 2). We observed three main firing patterns, which we categorically defined as type I (tonic firing), type II (paroxysmal bursting with a plateau potential at suprathreshold current injections beyond the peak of the *f-I* curve) and type III (rapid transition to a plateau potential ± bursting at/near rheobase during the rising phase of the *f-I* curve). We found that types II and III were more frequently observed among variant iNeurons versus control across time points (Fig. 4C; $P < 0.0001$ via chi-square test).

We then analysed the properties of individual APs, with a focus on electrophysiological measures known to depend on Na$^+$ current. We found that voltage threshold for AP generation was lower (more negative/hyperpolarized) in variant versus control iNeurons (Fig. 5A and B and Supplementary Table 1). APs were also wider (prolonged) in variant versus control iNeurons, as measured by AP half-width and APD$_{90}$ (Supplementary Fig. 8 and Supplementary Table 1). Given inherent variability across neurons, we also analysed the electrical excitability of variant iNeurons by type. We found that type III neurons had a
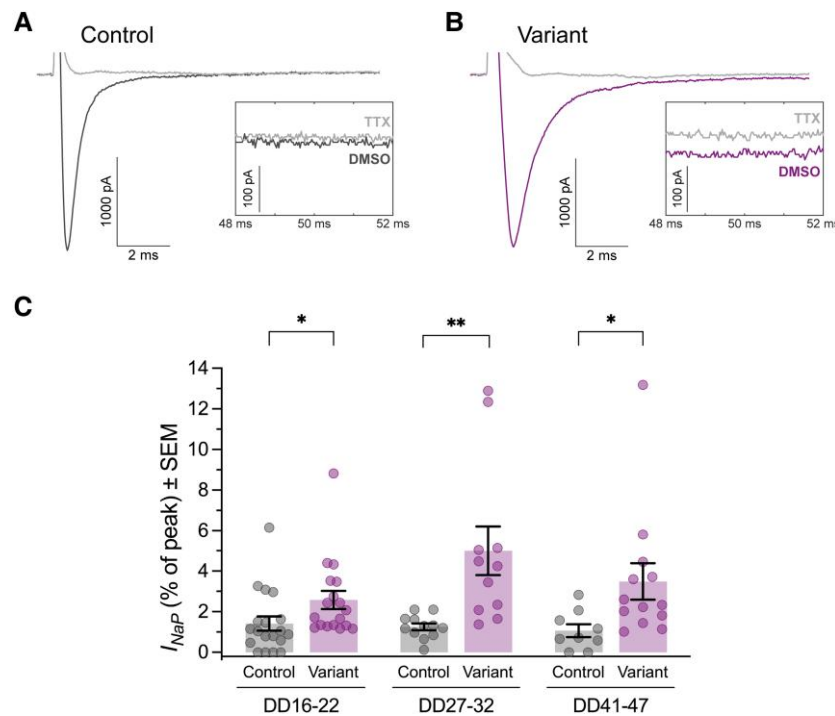
Figure 3 SCN3A-p.Ile875Thr iNeurons exhibit increased persistent Na$^+$ current relative to isogenic control. (A and B) Representative recordings showing inward Na$^+$ current and slowly-inactivating/persistent current (I_{NaP}) from control (**A**, dark grey) and variant iNeurons (**B**, purple) at differentiation day (DD)17 during local perfusion of vehicle (dimethyl sulphoxide, DMSO) followed by 500 nM tetrodotoxin (TTX, light grey) to block all Na$^+$ current. Na$^+$ currents were elicited by voltage steps to −10 mV from a holding potential of −90 mV. *Insets* show currents before and after TTX at 50 ms, where I_{NaP} was quantified. (**C**) Summary data demonstrating increased I_{NaP} in variant iNeurons relative to control. For each cell, I_{NaP} was calculated as the magnitude of TTX-sensitive current at 50 ms as a percentage of total peak transient inward Na$^+$ current at −10 mV. Shown are values from individual cells, with bars representing mean per condition ± standard error of the mean (SEM). *$P < 0.0332$; **$P < 0.0021$; ***$P < 0.0002$; ****$P < 0.0001$ by multiple Wilcoxon rank sum tests with Bonferroni-Dunn's multiple comparisons test to compare genotypes within each time window. n (control) = 19 (DD16–22), 12 (DD27–32), 9 (DD41–47); n (variant) = 18 (DD16–22), 11 (DD2732), 13 (DD41–47).

markedly lower AP threshold compared to type I at both DD16–22 and DD41–47 (Fig. 5C and Supplementary Table 3).

We additionally analysed properties of repetitive firing, again comparing variant to control as well as variant types to one another. Variant iNeurons exhibited higher (faster) firing rates compared to control at DD16–22, although this difference had normalized by DD41–47 (Fig. 5D and F and Supplementary Table 1). However, subgroup analysis revealed that type II neurons exhibited higher firing frequencies than type I, whereas type III neurons had markedly lower firing rates compared to types I and II, and these differences were evident at both time points (Fig. 5E and G and Supplementary Table 3). These results suggest that, while type II variant iNeurons are hyperexcitable relative to type I with respect to AP threshold and firing frequency, type III variant iNeurons present a mixed phenotype with a hyperpolarized AP threshold yet decreased firing frequency.

Recapitulation of cellular dysfunction in patient-derived iNeurons

To validate our findings in variant versus control iNeurons, we generated a separate iPSC line derived from a human patient harbouring the SCN3A-p.Ile875Thr variant. iPSCs were reprogrammed from patient peripheral blood mononuclear cells (PBMCs) to generate a patient-derived cell line (herein denoted 'Patient'). We then generated an isogenic control line using CRISPR/Cas9 gene editing in the patient-derived iPSCs to correct the pathogenic allele to wild-type (SCN3A c.2624, p.Ile875) (herein denoted 'Corrected').

Both patient and corrected iPSC lines were differentiated to iNeurons using the same Ngn2 induction protocol and iNeurons were recorded at the same time points as earlier (DD16–22, DD27–32 and DD41–47). Consistent with results in the variant versus control iNeurons, whole-cell voltage clamp recordings of Na$^+$ currents showed no genotype difference in peak transient Na$^+$ current density at any time point (Supplementary Fig. 5B), accompanied by increased I_{NaP} in patient compared to corrected iNeurons (Fig. 6A–C). We observed no genotype differences in voltage dependence of steady-state inactivation (Supplementary Fig. 6D–F) nor recovery from inactivation, with the exception of slightly impaired time course of recovery from inactivation in patient versus corrected iNeurons at DD41–47 (Supplementary Fig. 7D–F).

Using whole-cell current clamp recordings, we found that patient and corrected iNeurons exhibited the same firing pattern types as earlier (Fig. 6D and E and Supplementary Table 2), with a significantly greater proportion of aberrant type II and III observed in patient versus corrected iNeurons across time points (Fig. 6G; $P < 0.0001$ via chi-square test). Analysis of the properties of individual APs and repetitive firing in patient versus corrected iNeurons further recapitulated findings of the altered intrinsic excitability seen in variant versus control iNeurons. AP threshold was significantly lower (more negative/hyperpolarized) in patient iNeurons compared to corrected at all time points (Fig. 6F and H and Supplementary Table 4). AP halfwidth and APD$_{90}$ were also significantly wider (prolonged) at DD16–22 in patient iNeurons versus corrected (Supplementary Fig. 8D and Supplementary Table 4). Finally,
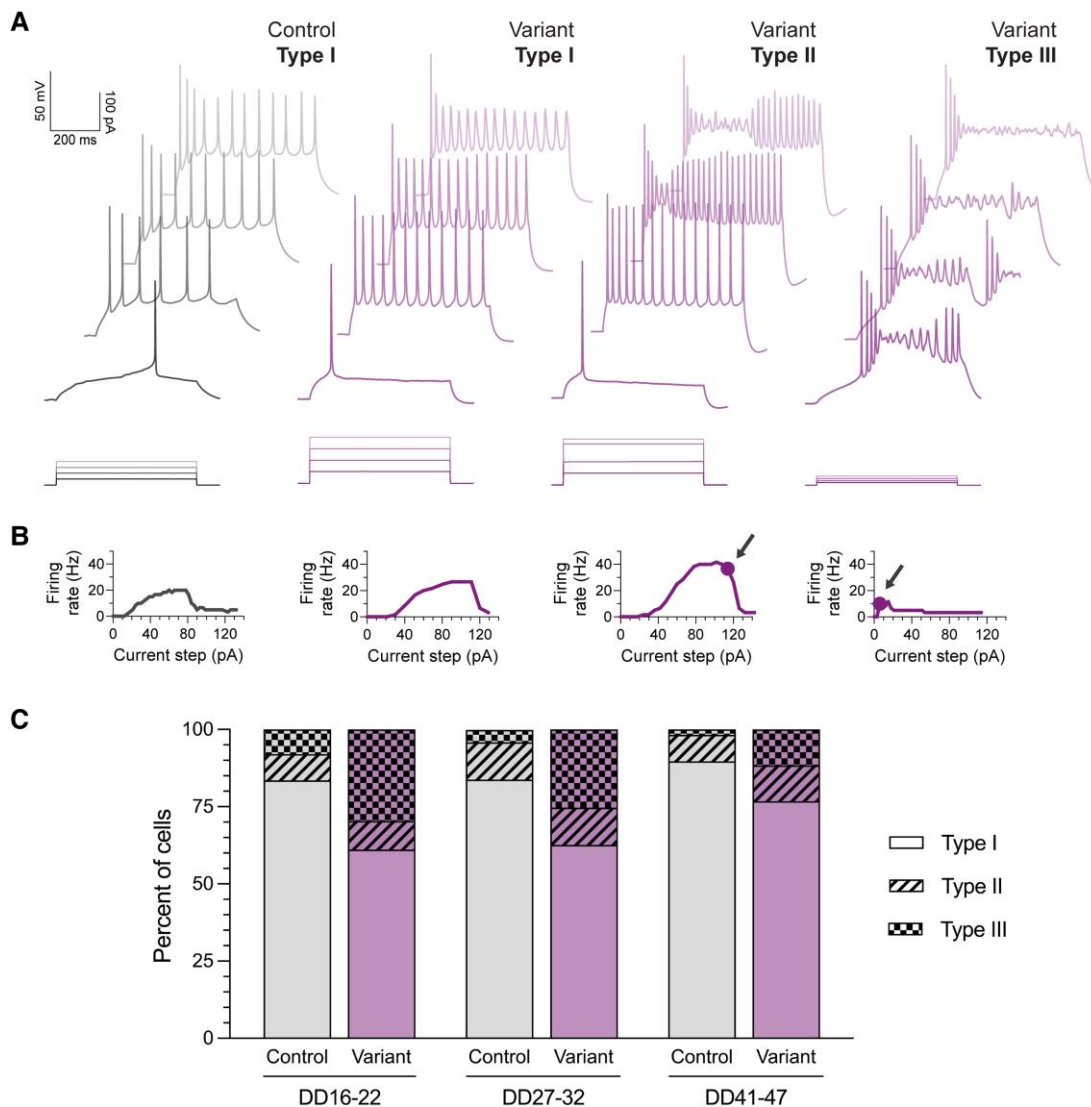
Figure 4 A prominent subset of SCN3A-p.Ile875Thr iNeurons exhibit aberrant firing patterns. (**A**) Representative recordings demonstrating firing patterns of control and variant iNeurons at differentiation day (DD)16–22 evoked by threshold (rheobase) and suprathreshold current injections. Firing patterns were categorically defined as type I (tonic firing), type II (paroxysmal bursting with a plateau potential at suprathreshold current injections beyond the peak of the *f-I* curve), and type III (rapid transition to a plateau potential $\pm$ bursting at/near rheobase during the rising phase of the *f-I* curve). Voltage responses corresponding to 1×, 2×, 3× and 4× rheobase are shown for each cell, with the exception of the variant type II example, which shows the ~3.5× rheobase response representing the first instance of a plateau-like event in that cell. Current injections corresponding to each voltage trace are shown at the *bottom*. Scale bar applies to all panels. (**B**) Current-firing rate (*f-I*) curves for the individual iNeurons shown in **A**. Bold circle with arrow indicates the first sweep at which a plateau-like event occurred in the variant type II and III neurons, highlighting the distinction between types. (**C**) Percentages of type I, II and III firing patterns observed in control and variant iNeurons at each recording time window. Comparing cells of each genotype combined across all time points, chi-square analysis reveals a significant association between genotype and firing type ($\chi^2 = 51.99$, df = 2, $P < 0.0001$). *n* (control) = 176 (DD16–22), 99 (DD27–32), 58 (DD41–47); *n* (variant) = 216 (DD16–22), 91 (DD27–32), 69 (DD41–47).

patient iNeurons exhibited higher (faster) firing rates compared to corrected at DD16–22, with this difference normalizing by DD41–47 (Fig. 6I and J).

Thus, patient iNeurons expressing the *SCN3A*-p.Ile875Thr variant on a different genetic background fully reproduce findings obtained using the variant versus control lines, including increased I_{NaP} and altered intrinsic excitability consistent with Na$^+$ channel dysfunction in patient versus corrected lines. We also compared variant versus patient and control versus corrected lines and found no differences at any time window in the key Na$^+$ channel-dependent biophysical parameters identified as altered between genotypes, such as AP threshold

and maximal steady-state firing frequency, further supporting a causative effect of the -p.Ile875Thr variant on these properties.

Correction of pathological activity with Na$_v$1.3-specific pharmacology

Finally, we tested whether blockade of Na$_v$1.3 could reverse the abnormal neuronal activity observed in iNeurons harbouring the *SCN3A*-p.Ile875Thr variant. We used the Na$_v$1.3-selective Na$^+$ channel blocker ICA-121431, which we previously used to validate the presence of functional Na$_v$1.3-containing channels in the iNeuron
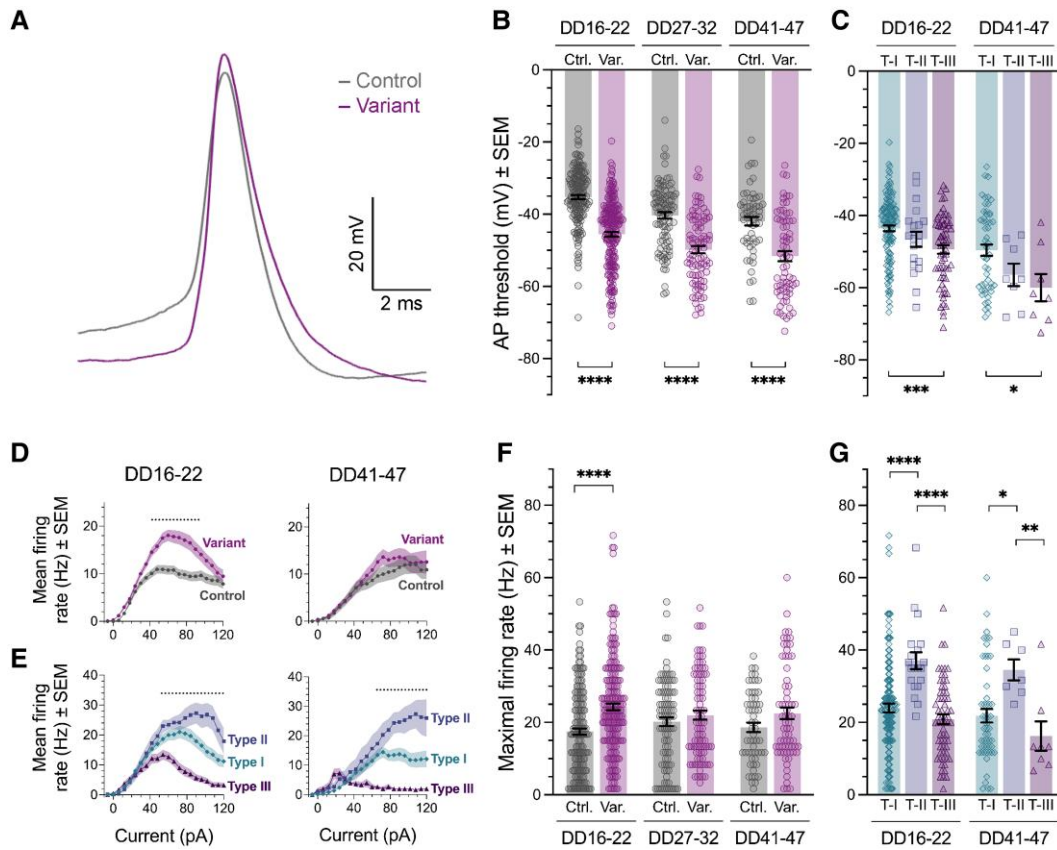
Figure 5 Altered intrinsic excitability in SCN3A-p.Ile875Thr iNeurons. (A) Representative example traces of single action potentials (APs) at differentiation day (DD)17 from a control (grey) and a variant (purple) iNeuron, aligned in time at peak and overlaid to demonstrate lowered (more hyperpolarized) AP threshold in variant (Var) iNeurons relative to control (Ctrl). **(B and C)** Variant iNeurons overall display a more hyperpolarized AP threshold compared to control at all time windows **(B)**, with type III (TIII) variant iNeurons exhibiting the most hyperpolarized AP threshold **(C)**. **(D and E)** Variant iNeurons overall exhibit higher evoked firing rates at a given current injection compared to control at DD16–22, but this effect has normalized by DD41–47 **(D)**. However, among variant iNeurons, the evoked firing rates of type II neurons are higher compared to type I at suprathreshold current injections, whereas the evoked firing rates of type III neurons are lower compared to type I **(E)**. Shown are average firing frequencies ± standard error of the mean (SEM) for each current injection. Dotted line indicates current injections with statistical significance across genotype or firing type via two-way ANOVA with Šídák multiple comparisons tests (in **D**, to compare genotypes at each current injection) or Tukey's multiple comparisons tests (in **E**, to compare firing types with each other at each current injection). In **(D)**, n (control) = 116 (DD16–22), 29 (DD41–47); n (variant) = 107 (DD16–22), 40 (DD41–47). In **E**, n (type I) = 60 (DD16–22), 30 (DD41–47); n (type II) = 13 (DD16–22), 5 (DD41–47); n (type III) = 34 (DD16–22), 5 (DD41–47). **(F and G)** Variant iNeurons display a higher maximal steady-state firing frequency compared to controls at DD16–22 **(F)**. However, among variant iNeurons, type II neurons exhibit higher maximal steady-state firing frequency compared to type I and type III neurons **(G)**. *$P < 0.0332$; **$P < 0.0021$; ***$P < 0.0002$; ****$P < 0.0001$; by multiple Wilcoxon rank sum tests with Bonferroni-Dunn's multiple comparisons test to compare genotypes within each time window in **B** and **F**, and by Kruskal-Wallis test with Dunn's multiple comparisons test to compare firing types within each time window in **C** and **G**. Shown are values from individual cells, with bars representing mean per condition ± SEM. n (control) = 176 (DD16–22), 99 (DD27–32), 58 (DD41–47); n (variant) = 216 (DD16–22), 91 (DD27–32), 69 (DD41–47).

system and found to partially block increased I_{NaP} in variant iNeurons at submicromolar concentrations (Fig. 2).

We found that 20 nM ICA-121431 reversibly decreased firing frequency in control as well as variant type I iNeurons (Fig. 7A and C), consistent with action as a Na⁺ channel blocker. However, in variant type III neurons, 20 nM ICA-121431 blocked the plateau potential-like events and exerted a net increase in firing frequency, effectively converting type III neurons to a type I firing pattern (Fig. 7B and C). This effect was reversible, as we observed a return of plateau events following washout of ICA-121431 (Fig. 7B).

We also studied the effect of ICA-121431 on the properties of individual APs. In control iNeurons, 20 nM ICA-121431 had no effect on AP threshold compared to vehicle (dimethyl sulphoxide, DMSO) (Fig. 7D). However, 20 nM ICA-121431 normalized (increased) AP threshold in variant iNeurons, across firing types I, II and III (Fig. 7D). We also found that 20 nM ICA-121431 decreased

AP amplitude and shortened AP half-width of variant iNeurons to control levels (Supplementary Fig. 9).

Discussion

Voltage-gated sodium (Na⁺) channels are macromolecular complexes that underlie the generation and propagation of APs and hence are critical regulators of neuronal excitability. *SCN3A* encodes the voltage gated Na⁺ channel α subunit Na$_v$1.3, which is highly expressed in developing brain. *SCN3A*-related neurodevelopmental disorders (*SCN3A*-NDDs) constitute a clinical spectrum of disease that includes epilepsy and/or MCD typically accompanied by developmental delay/intellectual disability of variable degree but frequently of a severe to profound extent. How variation in *SCN3A* leads to these associated disease manifestations is unknown. Here, we use an iPSC-derived iNeuron *in vitro* model of developing cortical neurons to investigate pathomechanisms
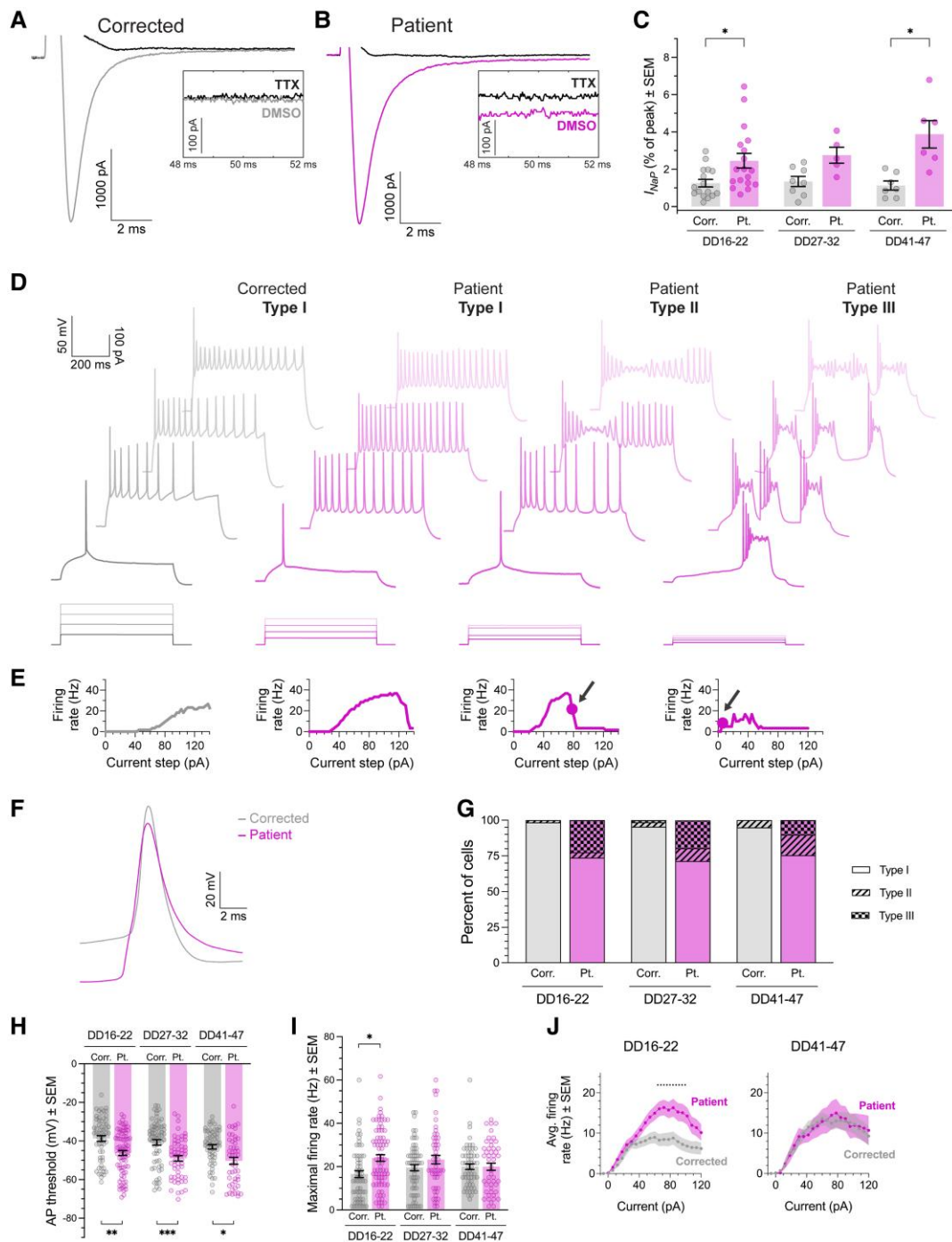
Figure 6 Recapitulation of increased I_{NaP}, firing abnormalities and altered intrinsic excitability in iNeurons derived from an SCN3A-p.Ile875Thr patient line. (A and B) Representative recordings showing inward Na^+ current and I_{NaP} from corrected (Corr.) (A, grey) and patient (Pt.) (B, magenta) iNeurons at differentiation day (DD)17 in vehicle (dimethyl sulphoxide, DMSO) followed by 500 nM tetrodotoxin (TTX, black). Na^+ currents were elicited by depolarization to −10 mV from a −90 mV holding potential. Insets show currents before/after TTX at 50 ms. (C) Summary data. Increased I_{NaP} in patient iNeurons relative to corrected. As in Fig. 3, I_{NaP} was quantified as the TTX-sensitive current at 50 ms as a percentage of transient inward Na^+ current at −10 mV. Shown are values from individual cells, with bars representing mean ± standard error of the mean (SEM). *$P < 0.0332$; **$P < 0.0021$; ***$P < 0.0002$; ****$P < 0.0001$; by multiple Wilcoxon ranked sum tests with Bonferroni-Dunn's multiple comparisons test. n (corrected) = 16 (DD16–22), 8 (DD27–32), 7 (DD41–47); n (patient) = 18 (DD16–22), 5 (DD27–32), 6 (DD41–47). (D) Firing patterns of corrected and patient iNeurons at DD16–22 evoked by threshold (rheobase) and suprathreshold current injections. As in Fig. 4, firing patterns were categorically defined as type I–III. Voltage responses corresponding to 1×, 2×, 3× and 4× rheobase are shown for each cell, with the exception of the patient type II example, which shows ~3.5× rheobase as the first instance of a plateau-like event in that cell. Current injections corresponding to each voltage trace are shown at the bottom; scale bar applies to all panels. (E) f-I curves for the individual iNeurons shown in D. Bold circle with arrow indicates the first sweep at which a plateau-like event occurred in the patient type II and III neurons. (F) Representative example traces of single action potentials (APs) at DD17 from a corrected (grey) and patient (magenta) iNeuron, aligned at peak and overlaid to demonstrate markedly hyperpolarized AP threshold in patient iNeurons. (G) Percentages

(continued)

of *SCN3A*-NDD, focusing on the most common recurrent disease-associated variant *SCN3A*-p.Ile875Thr.

Genotype-phenotype correlations

All reported patients with the recurrent c.2624T>C; p.Ile875Thr variant exhibit a consistent phenotype, including neonatal-onset treatment-resistant epilepsy, severe-to-profound neurocognitive impairment and diffuse polymicrogyria (PMG).[1,2,6,8] We previously found that Na$^+$ channels containing Na$_v$1.3-p.Ile875Thr variant subunits exhibit gain of ion channel function (GoF) with a leftward/hyperpolarized shift in the voltage dependence of channel activation and increased persistent current (I_{NaP}).[1,2] Here, we extend these findings to show that iNeurons harbouring the recurrent heterozygous *SCN3A* c.2624T>C (p.Ile875Thr) variant also exhibit increased I_{NaP}. Of note, we found I_{NaP} to be 1.5%–4% of transient/total inward Na$^+$ current in *SCN3A*-p.Ile875Thr iNeurons, whereas we recorded 10.9 ± 1.6% I_{NaP} in heterologous systems.[1,2] This discrepancy can likely be accounted for by the fact that the *SCN3A*-p.Ile875Thr variant exists in a heterozygous state in iNeurons, as well as the fact that Na$_v$1.3-containing Na$^+$ channels constitute only a portion of total Na$^+$ current in iNeurons, which we also confirmed express *SCN2A* transcripts (encoding Na$_v$1.2). The fact that we found no differences between variant versus patient and control versus corrected lines in the key biophysical parameters identified as altered between genotypes (AP threshold, maximal steady-state firing frequency) further supports the causative/dominant effect of the variant as determinant of the observed differences in intrinsic excitability. Hence, while we cannot rule out some role of genetic background in determining the intrinsic excitability of different lines, we consider the identified differences to be largely or entirely attributable to the *SCN3A*-p.Ile875Thr variant, consistent with the established basis of the disease as due to the heterozygous variant arising *de novo*.

While the iNeuron system is less favourable for the detailed biophysical characterization of Na$^+$ currents as compared to heterologous cells such as HEK-293T, our approach uniquely facilitates the recording of native Na$^+$ currents in human neurons. We rejected from analysis any iNeuron that exhibited an escape action potential (which was observed in a subset of cells in response to step depolarization to 0 mV or above). We confirmed that time to peak of the Na$^+$ currents recorded in iNeurons at room temperature was equivalent to that in heterologously expressed Na$_v$1.3 in HEK-293T cells. An alternative approach towards achieving improved space clamp in iNeurons is the use of outside-out nucleated macropatches,[40] although it is unclear if this approach would sample the same population or distribution of Na$^+$ channels as whole-cell recordings.

In our prior study,[2] we found that variants identified in *SCN3A*-NDD patients with an epileptic encephalopathy phenotype formed Na$^+$ channels that largely exhibited GoF. We also found that Na+ channels formed by variant Na$_v$1.3 subunits corresponding

to patients with MCD uniformly exhibited GoF, although in some patients this was quite modest (3%–5% I_{NaP} compared to peak transient I_{Na}). However, not all patients with *SCN3A*-NDD and epileptic encephalopathy have MCD, suggesting that epilepsy in *SCN3A*-NDD is not primarily driven by brain malformation. The median age of onset of epilepsy in *SCN3A*-NDD patients with MCD is 2 weeks, similar to the age of onset of *SCN3A*-NDD patients with epileptic encephalopathy without MCD,[2,9] whereas the median age of epilepsy onset in patients with PMG and epilepsy is ~3 years.[41] Furthermore, not all variants exhibiting profound GoF correspond to patients with MCD; we showed that a large increase in I_{NaP} alone was insufficient to produce MCD, as the recurrent variant *SCN3A*-p.Val1769Ala seen in three patients with *SCN3A*-NDD exhibited a very large persistent current (~30% of peak transient) and clinically was associated with severe/profound global impairment and treatment-resistant epilepsy yet without MCD.[1,2] Why GoF variants are not associated with MCD in all cases remains unclear.

Insight into disease pathomechanisms

Increased I_{NaP} is known to be linked to epilepsy,[42,43] has been identified as an effect of epilepsy-associated variants in all other brain-expressed Na$^+$ channels *SCN1A*, *SCN2A* and *SCN8A*,[4,44,45] and has also been identified in variants ascertained in patients with other Na$^+$ channelopathies, including periodic paralysis,[46] cardiac arrhythmia[47,48] and pain disorders.[49] Hence, it is not unexpected that some proportion of epilepsy-associated variants in *SCN3A*, which is known to be expressed widely in developing cerebral cortex, might also act at least in part via elevated I_{NaP}. Increased I_{NaP} is generally thought to increase neuronal excitability. For example, clear hyperexcitability has been observed in iPSC-derived neurons generated from patients with *SCN8A* encephalopathy who harbour pathogenic variants that give rise to Na$_v$1.6-containing Na$^+$ channels with increased I_{NaP}.[12] The apparent hyperpolarized voltage threshold for AP generation, increased firing rate and paroxysmal bursting behaviour that we observed in iNeurons generated from *SCN3A*-p.Ile875Thr-expressing lines are consistent with a GoF effect of increased I_{NaP}.

However, we also observed elements suggesting potential loss-of-function (LoF) in iNeurons, particularly the decreased firing rate in type III *SCN3A*-p.Ile875Thr iNeurons relative to controls. We attribute this reduced firing frequency in type III iNeurons to the plateau potential-like events that define this firing type. Apparently accelerated transition to plateau potentials is consistent with enhanced Na$^+$ current due to increased I_{NaP} that drives the cell into plateau/early depolarization block, which is likely best represented quantitatively in the increased (prolonged) APD$_{90}$ observed in *SCN3A*-p.Ile875Thr iNeurons. That increased I_{NaP} could act to generate decreased excitability or a mixed pattern of gain/loss-of-function at the level of neuronal excitability has been reported previously.[50-52] Such work illustrates that the GoF/LoF dichotomy can be an oversimplification,[53] as highlighted by our

Figure 6 (Continued)
of type I, II and III firing patterns observed in corrected and patient iNeurons. Comparing cells of each genotype combined across all time points, chi square analysis reveals a significant association between genotype and firing type ($\chi^2 = 40.59$, df = 2, $P < 0.0001$). (**H** and **I**) Compared to corrected iNeurons, patient iNeurons display a more hyperpolarized AP threshold at all time windows (**H**) and higher maximal steady-state firing frequency at DD16–22 (**I**). (**J**) Patient iNeurons exhibit higher evoked firing rates at a given current injection compared to corrected at DD16–22, which normalizes by DD41–47. Shown are average firing frequencies ± standard error of the mean (SEM) at each current injection. Dotted line indicates current injections with statistical significance across genotype via two-way ANOVA with Šídák multiple comparisons test to compare genotypes at each current injection. n (corrected) = 35 (DD16–22), 21 (DD41–47); n (patient) = 43 (DD16–22), 12 (DD41–47). (**G–I**), n (corrected) = 61 (DD16–22), 65 (DD27–32), 59 (DD41–47); n (patient) = 80 (DD16–22), 56 (DD27–32), 49 (DD41–47). (**H** and **I**) Values from individual cells are shown, with bars representing mean per condition ± SEM. *$P < 0.0332$; **$P < 0.0021$; ***$P < 0.0002$; ****$P < 0.0001$; by multiple Wilcoxon rank sum tests with Bonferroni-Dunn's multiple comparisons test.
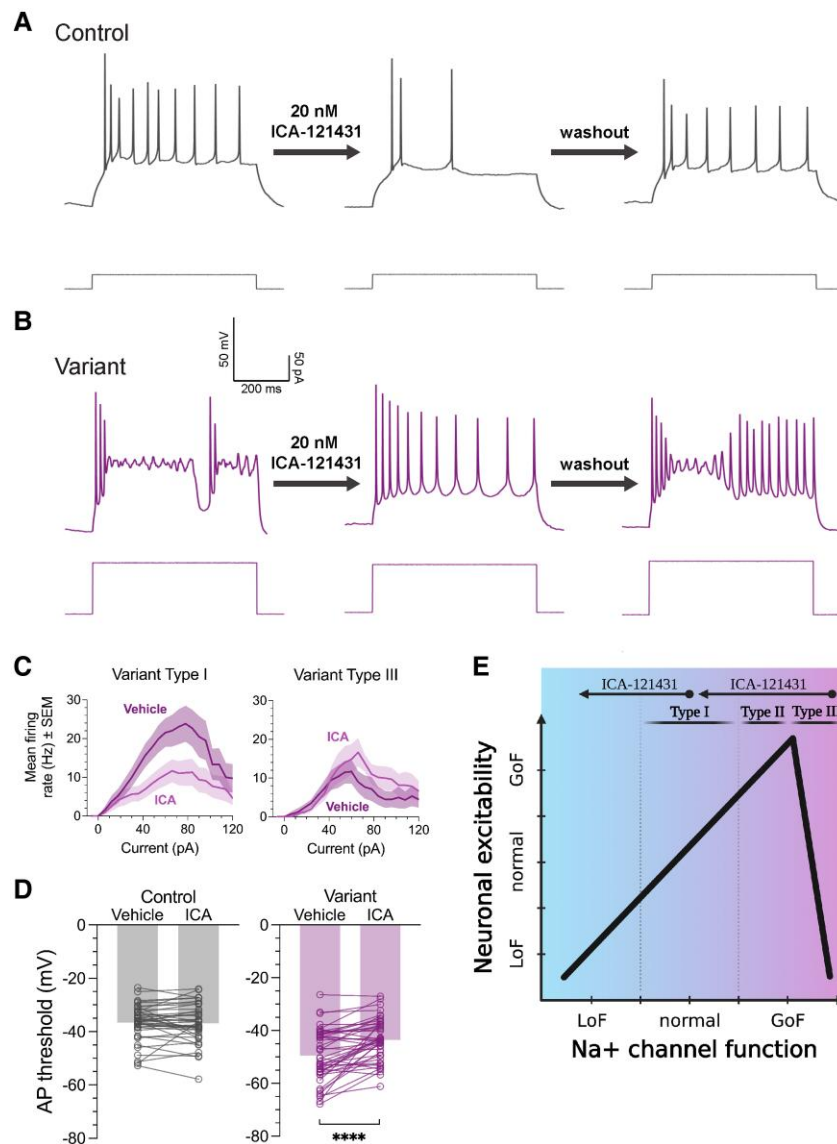
Figure 7 Na$_v$1.3-specific blocker ICA-121431 corrects aberrant firing and excitability in variant iNeurons. (A and B) Example recordings of iNeurons in the differentiation day (DD)16–22 window in response to an identical current injection before, during and after (washout) application of 20 nM ICA-121431. In control (**A**), ICA-121431 reversibly reduced excitability of a type I iNeuron, as indicated by firing frequency. In variant (**B**), a type III paroxysmal firing pattern was reversibly normalized by ICA-121431. Scale bar applies to both panels. (**C**) Subtype analysis of variant neurons reveals opposing effects of 20 nM ICA-121431 on current-firing (f-I) relationships. In type I variant neurons, ICA-121431 results in a trend toward decreased firing frequency per current injection, whereas ICA-121431 appears to selectively increase firing frequency at higher current injections in type III variant iNeurons. Two-way ANOVA with Šídák multiple comparisons test revealed no current injections with statistical significance across treatment condition for either type I or type III. n (type I) = 13, n (type III) = 10. (**D**) Application of 20 nM ICA-121431 raises action potential (AP) threshold in variant iNeurons at DD16–22, with no net effect in controls. Shown are values from individual cells with bars representing mean per condition. $^*P < 0.0332$; $^{**}P < 0.0021$; $^{***}P < 0.0002$; $^{****}P < 0.0001$; by two-tailed paired t-test. n (control) = 42, n (variant) = 47. (**E**) A working model of how gain- or loss-of-function of Na$_v$1.3-containing Na$^+$ channels result in changes in neuronal function. This model explains the phenotypic variability observed in iNeurons and provides a biological basis for the categorical difference between type II and type III neurons. Whether Na$^+$ channel blockade by ICA-121431 results in increased or decreased excitability depends on neuronal firing type, which is hypothesized to depend on the presence or absence of a pathogenic variant in SCN3A as well as overall SCN3A expression levels. Created with BioRender.com. GoF = gain-of-function; LoF = loss-of-function; SEM = standard error of the mean.

finding here in iNeurons that heterozygous expression of a variant that exerts GoF at the ion channel level results in more complex effects at the level of neuronal excitability. We propose a working model whereby Na$^+$ channel function and neuronal excitability—each existing on a spectrum from LoF to normal to GoF—have a direct relationship up to a critical point beyond which further Na+ channel GoF (e.g. I_{NaP}) results in decreased neuronal function (e.g. as manifested in firing rate) (Fig. 7E). This model offers a biological explanation for the difference between the categorically defined type II and III firing patterns of SCN3A-p.Ile875Thr neurons (Fig. 7E). Our work further shows the power of the iNeuron system for the study of epilepsy[54] and the importance of studying epilepsies across a range of models. That said, recent work shows that LoF of Scn2a (associated with autism spectrum disorder) in mouse leads to an apparent increase in neuronal excitability of Na$_v$1.2-expressing neocortical pyramidal cells at adult time

points.[55,56] We consider such plasticity mechanisms to be unlikely to occur in the iNeuron system, which models prenatal neuronal development.[23] Consistent with this interpretation, Que *et al.*[57] show that human iNeurons from a patient with epileptic encephalopathy due to the variant SCN2A-p.Leu1342Pro exhibit features of GoF at the level of endogenous Na$^+$ currents and cellular and network excitability *in vitro*. Recent work has used multi-electrode array (MEA) approaches to attempt to link the excitability of individual iNeurons to network activity *in vitro*.[12,13,58] Future work evaluating the SCN3A-p.Ile875Thr iPSC lines using MEA or organoid systems, or a mouse model of SCN3A encephalopathy, could further inform the question of how the neuronal dysfunction observed here might manifest at the level of circuits or intact brain.

Abnormal excitability was only noted in a subset of iNeurons from both lines harbouring the SCN3A-p.Ile875Thr variant. Why this is the case is not clear but may be due to varying levels of Na$_v$1.3 expression between cells. It is known that the level of SCNXA mRNA, even between neurons of a genetically-defined cell type, varies widely in mouse and human[59-62] and we did observe a variable proportion of ICA-121431-sensitive current between cells. Furthermore, single cell expression profiling and transcriptomic analyses of neurons induced by Ngn2 overexpression have reported varying degrees of molecular heterogeneity.[23,39,63] Thus, it is possible that, among SCN3A-p.Ile875Thr iNeurons, a greater proportion of Na$_v$1.3-mediated Na$^+$ current results in aberrant excitability (i.e. type II and III firing patterns), whereas a greater proportion of Na+ current mediated by other wild-type Na$^+$ channels (likely Na$_v$1.2, based on our RT-qPCR data), can nonetheless produce near-normal firing patterns (i.e. type I). A different approach, such as single-cell RNASeq, would be required to directly compare Na$^+$ channel transcript levels between cells; PatchSeq might further allow correlation of Na$^+$ channel transcripts with specific firing patterns. However, it remains the case that transcript levels do not necessarily equate to protein levels, as has been shown specifically for Na+ channels in iNeuron systems.[10]

Regarding mechanisms underlying MCD in SCN3A-NDD, this study offers little additional insight. It is possible that plateau potentials driven by abnormal electrical excitability due to increased I$_{NaP}$, as we observed in iNeurons from SCN3A-p.Ile875Thr lines, could produce alteration of the resting membrane potential and/or abnormal calcium signalling in intermediate progenitors and developing neurons of the embryonic human brain. Such alterations could lead to abnormal cell cycle regulation and/or migration and post-migratory integration of early neurons into developing cerebral cortex.[64,65] Because we considered the possibility that the SCN3A variant might influence the rate of developmental maturation of iNeurons, we applied a less stringent set of inclusion criteria related to resting membrane potential (at or below/more hyperpolarized than −30 mV; see the 'Materials and methods' section) than some studies,[12,13,22] which likely contributed to the variability we observed between cells (as has been observed by other groups[38,58,66,67]).

Towards a potential targeted therapy

Our prior work[1,2] integrated data from multiple collaborators across an international patient cohort, yet information on best treatments for epilepsy in SCN3A-NDD did not emerge. Of 15 patients for whom detailed clinical data were available, six were treated at some point with anti-seizure drugs with Na$^+$ channel blockade as the prominent mechanism of action (oxcarbazepine, lamotrigine, lacosamide and/or phenytoin). It remains possible that early initiation of Na$^+$

channel blockers (perhaps at high doses), or of an Na$_v$1.3-specific agent, could be an effective therapy for epilepsy associated with SCN3A-NDD. Furthermore, it is possible that such treatment would only be required for a delimited time period given that expression of SCN3A decreases during development. However, epilepsy persists in many patients with SCN3A-NDD long beyond Na$_v$1.3 is thought to be downregulated, suggesting that chronic impairment might be driven by abnormal excitability during early development and/or by hyperexcitability due to structural brain abnormality. Although we saw evidence of downregulation of SCN3A in our iNeuron system (with no upregulation of SCN1A) by DD42 via RT-qPCR, we observed genotype differences in electrophysiological phenotypes at all three time windows and did not observe a difference between DD28 and DD42 time points when compared within lines. However, given the cell-to-cell variability within a given time point, it may be difficult to comment on this with certainty. This general issue may be better addressed in a mouse model.

In this study, we used the compound ICA-121431, which acts as a gating inhibitor with relative selectivity for Na$_v$1.3-containing Na$^+$ channels with a reported IC$_{50}$ of 18 ± 5 nM in heterologous systems.[25] We first used this compound to show that iNeurons in our experimental system express Na$_v$1.3, a conclusion also supported by results of RT-qPCR and the observation itself that SCN3A-p.Ile875Thr iNeurons exhibited abnormal Na$^+$ currents and intrinsic excitability. Although ICA-121431 also blocks Na$_v$1.1-containing Na$^+$ channels with a similar IC$_{50}$ in heterologous systems, we showed that iNeurons express little/no SCN1A transcript via RT-qPCR, nor functional Na$_v$1.1-mediated Na$^+$ channels based on a lack of effect of the Na$_v$1.1 selective activator Hm1a[35] on I$_{Na}$ recorded from iNeurons. We found that ICA-121431 at submicromolar concentrations blocked a similar proportion of transient and persistent Na$^+$ current in iNeurons and normalized aberrant excitability, including altered AP threshold, paroxysmal bursting and plateau potentials seen in SCN3A-p.Ile875Thr iNeurons. It is seemingly paradoxical that application of a Na$^+$ channel blocker could increase neuronal excitability. However, we found this effect to be selective to the most severely abnormal type III SCN3A-p.Ile875Thr iNeurons, whereas ICA-121431 decreased excitability of control and type I variant iNeurons by decreasing firing rate, as would be expected of blocking a proportion of a neuron's voltage-gated Na$^+$ channels. Mapping this finding onto our working model offers an explanation for the seemingly contradictory actions of ICA-121431 (Fig. 7E). Further development of an Na$_v$1.3-specific compound (with no activity against Na$_v$1.1-containing Na$^+$ channels) could have clinical utility for SCN3A epilepsy. It should be noted that van Hugte *et al.*[58] recently showed evidence of altered neuronal and network excitability at DD49 in iNeurons generated from iPSCs from patients with Dravet syndrome via the same rapid Ngn2 protocol, suggesting the potential expression of Na$_v$1.1 in developing pyramidal cells at this later time point *in vitro* and/or alterations in the expression of other ion channels.

Limitations

The major limitation of this work is the lack of insight provided into mechanisms of MCD, although it is the case that a prominent subset of patients with SCN3A-NDD exhibit severe epilepsy without MCD. While we establish that the Ngn2 iNeuron system rapidly generates electrically active neurons with functional Na$_v$1.3-containing Na$^+$ channels, providing a suitable model for studying the physiological effects of pathogenic variants in SCN3A, it is

possible that this protocol bypasses developmental stages relevant to MCD pathogenesis. A small molecule, dual-SMAD inhibition directed differentiation paradigm, which better recapitulates human brain development *in vitro* by guiding iPSCs through a neural progenitor cell (NPC) stage into cortical neurons may provide more insight into mechanisms of MCD, as has been reported in relevant neurodevelopmental disorders such as ASD with macrocephaly.[68] Future work using alternative systems, such as human cerebral organoids,[69,70] mouse models or gyrencephalic animals, such as ferret[6,71] or marmoset,[72] could further advance our understanding of how pathogenic variants in *SCN3A* lead to brain malformation.

Data availability

Supporting data for the experiments performed in this study can be found in the Supplementary material and will be made available in the Goldberg Lab data repository (https://gin.g-node.org/GoldbergNeuroLab).

Acknowledgements

Funding

Competing interests

The authors report no competing interests.

Supplementary material

Supplementary material is available at *Brain* online.

References

1. Zaman T, Helbig I, Božović IB, et al. Mutations in SCN3A cause early infantile epileptic encephalopathy. *Ann Neurol*. 2018;83:703-717.
2. Zaman T, Helbig KL, Clatot J, et al. SCN3A-Related neurodevelopmental disorder: A spectrum of epilepsy and brain malformation. *Ann Neurol*. 2020;88:348-362.
3. Claes L, Del-Favero J, Ceulemans B, Lagae L, Van Broeckhoven C, De Jonghe P. De novo mutations in the sodium-channel gene SCN1A cause severe myoclonic epilepsy of infancy. *Am J Hum Genet*. 2001;68:1327-1332.
4. Wolff M, Johannesen KM, Hedrich UBS, et al. Genetic and phenotypic heterogeneity suggest therapeutic implications in SCN2A-related disorders. *Brain*. 2017;140:1316-1336.
5. Larsen J, Carvill GL, Gardella E, et al. The phenotypic spectrum of SCN8A encephalopathy. *Neurology*. 2015;84:480-489.
6. Smith RS, Kenny CJ, Ganesh V, et al. Sodium channel SCN3A (NaV1.3) regulation of human cerebral cortical folding and oral motor development. *Neuron*. 2018;99:905-913.e7.
7. Inuzuka LM, Macedo-Souza LI, Della-Ripa B, et al. Neurodevelopmental disorder associated with de novo SCN3A pathogenic variants: Two new cases and review of the literature. *Brain Dev*. 2020;42:211-216.
8. Miyatake S, Kato M, Sawaishi Y, et al. Recurrent SCN3A p.Ile875Thr variant in patients with polymicrogyria. *Ann Neurol*. 2018;84:159-161.
9. Helbig KL, Goldberg EM. SCN3A-related neurodevelopmental disorder. In: Adam MP, Feldman J, Mirzaa GM, et al., eds. *GeneReviews®*. University of Washington, Seattle; 2021.
10. Liu Y, Lopez-Santiago LF, Yuan Y, et al. Dravet syndrome patient-derived neurons suggest a novel epilepsy mechanism. *Ann Neurol*. 2013;74:128-139.
11. Sun Y, Paşca SP, Portmann T, et al. A deleterious Nav1.1 mutation selectively impairs telencephalic inhibitory neurons derived from Dravet syndrome patients. *eLife*. 2016;5:e13073.
12. Tidball AM, Lopez-Santiago LF, Yuan Y, et al. Variant-specific changes in persistent or resurgent sodium current in SCN8A-related epilepsy patient-derived neurons. *Brain*. 2020;143:3025-3040.
13. Simkin D, Marshall KA, Vanoye CG, et al. Dyshomeostatic modulation of Ca2+-activated K+ channels in a human neuronal model of KCNQ2 encephalopathy. *eLife*. 2021;10:e64434.
14. Ricciardi S, Ungaro F, Hambrock M, et al. CDKL5 Ensures excitatory synapse stability by reinforcing NGL-1–PSD95 interaction in the postsynaptic compartment and is impaired in patient iPSC-derived neurons. *Nat Cell Biol*. 2012;14:911-923.
15. Yamashita S, Chiyonobu T, Yoshida M, et al. Mislocalization of syntaxin-1 and impaired neurite growth observed in a human iPSC model for STXBP1-related epileptic encephalopathy. *Epilepsia*. 2016;57:e81-e86.
16. Felts PA, Yokoyama S, Dib-Hajj S, Black JA, Waxman SG. Sodium channel alpha-subunit mRNAs I, II, III, NaG, Na6 and hNE (PN1): Different expression patterns in developing rat nervous system. *Brain Res Mol Brain Res*. 1997;45:71-82.
17. Beckh S, Noda M, Lübbert H, Numa S. Differential regulation of three sodium channel messenger RNAs in the rat central nervous system during development. *EMBO J*. 1989;8:3611-3616.
18. Suzuki H, Beckh S, Kubo H, et al. Functional expression of cloned cDNA encoding sodium channel III. *FEBS Lett*. 1988;228:195-200.
19. Liang L, Fazel Darbandi S, Pochareddy S, et al. Developmental dynamics of voltage-gated sodium channel isoform expression in the human and mouse brain. *Genome Med*. 2021;13:135.
20. Heighway J, Sedo A, Garg A, et al. Sodium channel expression and transcript variation in the developing brain of human, Rhesus monkey, and mouse. *Neurobiol Dis*. 2022;164:105622.
21. Busskamp V, Lewis NE, Guye P, et al. Rapid neurogenesis through transcriptional activation in human stem cells. *Mol Syst Biol*. 2014;10:760.
22. Rosa F, Dhingra A, Uysal B, et al. In vitro differentiated human stem cell-derived neurons reproduce synaptic synchronicity arising during neurodevelopment. *Stem Cell Reports*. 2020;15:22-37.
23. Nehme R, Zuccaro E, Ghosh SD, et al. Combining NGN2 programming with developmental patterning generates human excitatory neurons with NMDAR-mediated synaptic transmission. *Cell Rep*. 2018;23:2509-2523.
24. Zhang Y, Pak C, Han Y, et al. Rapid single-step induction of functional neurons from human pluripotent stem cells. *Neuron*. 2013;78:785-798.

25. McCormack K, Santos S, Chapman ML, et al. Voltage sensor interaction site for selective small molecule inhibitors of voltage-gated sodium channels. *Proc Natl Acad Sci U S A*. 2013; 110:E2724-E2732.

26. Maguire JA, Cardenas-Diaz FL, Gadue P, French DL. Highly efficient CRISPR/Cas9 mediated genome editing in human pluripotent stem cells. *Curr Protoc Stem Cell Biol*. 2019;48:e64.

27. Maguire JA, Gadue P, French DL. Highly efficient CRISPR/Cas9-mediated genome editing in human pluripotent stem cells. *Current Protocols*. 2022;2:e590.

28. Yang W, Mills JA, Sullivan S, Liu Y, French DL, Gadue P. iPSC reprogramming from human peripheral blood using sendai virus mediated gene transfer. In: *Stembook*. Harvard Stem Cell Institute; 2008.

29. Simkin D, Papakis V, Bustos BI, et al. Homozygous might be hemizygous: CRISPR/Cas9 editing in iPSCs results in detrimental on-target defects that escape standard quality controls. *Stem Cell Reports*. 2022;17:993-1008.

30. Li J, Ryan SK, Deboer E, et al. Mitochondrial deficits in human iPSC-derived neurons from patients with 22q11.2 deletion syndrome and schizophrenia. *Transl Psychiatry*. 2019;9:1-10.

31. Whitaker WR, Clare JJ, Powell AJ, Chen YH, Faull RL, Emson PC. Distribution of voltage-gated sodium channel alpha-subunit and beta-subunit mRNAs in human hippocampal formation, cortex, and cerebellum. *J Comp Neurol*. 2000;422:123-139.

32. Cheah CS, Westenbroek RE, Roden WH, et al. Correlations in timing of sodium channel expression, epilepsy, and sudden death in Dravet syndrome. *Channels (Austin)*. 2013;7:468-472.

33. Pollen AA, Nowakowski TJ, Chen J, et al. Molecular identity of human outer radial glia during cortical development. *Cell*. 2015;163:55-67.

33. 2010 Allen Institute for Brain Science. BrainSpan Atlas of the Developing Human Brain. Available from: http://brainspan.org

34. Osteen JD, Herzig V, Gilchrist J, et al. Selective spider toxins reveal a role for the Nav1.1 channel in mechanical pain. *Nature*. 2016;534:494-499.

35. Osteen JD, Sampson K, Iyer V, Julius D, Bosmans F. Pharmacology of the Nav1.1 domain IV voltage sensor reveals coupling between inactivation gating processes. *Proc Natl Acad Sci U S A*. 2017;114:6836-6841.

36. Moody WJ, Bosma MM. Ion channel development, spontaneous activity, and activity-dependent development in nerve and muscle cells. *Physiol Rev*. 2005;85:883-941.

37. Shih PY, Kreir M, Kumar D, et al. Development of a fully human assay combining NGN2-inducible neurons co-cultured with iPSC-derived astrocytes amenable for electrophysiological studies. *Stem Cell Res*. 2021;54:102386.

38. Schörnig M, Ju X, Fast L, et al. Comparison of induced neurons reveals slower structural and functional maturation in humans than in apes. *eLife*. 2021;10:e59323.

39. Asadollahi R, Delvendahl I, Muff R, et al. Pathogenic SCN2A variants cause early-stage dysfunction in patient-derived neurons. *Hum Mol Genet*. 2023;32:2192-2204.

40. Shain C, Ramgopal S, Fallil Z, et al. Polymicrogyria-associated epilepsy: A multicenter phenotypic study from the epilepsy phenome/genome project. *Epilepsia*. 2013;54:1368-1375.

41. Wengert ER, Patel MK. The role of the persistent sodium current in epilepsy. *Epilepsy Curr*. 2021;21:40-47.

42. Stafstrom CE. Persistent sodium current and its role in epilepsy. *Epilepsy Curr*. 2007;7:15-22.

43. Berecki G, Bryson A, Terhag J, et al. SCN1A Gain of function in early infantile encephalopathy. *Ann Neurol*. 2019;85:514-525.

44. Veeramah KR, O'Brien JE, Meisler MH, et al. De novo pathogenic SCN8A mutation identified by whole-genome sequencing of a

family quartet affected by infantile epileptic encephalopathy and SUDEP. *Am J Hum Genet*. 2012;90:502-510.

45. Lossin C, Nam TS, Shahangian S, et al. Altered fast and slow inactivation of the N440K Nav1.4 mutant in a periodic paralysis syndrome. *Neurology*. 2012;79:1033-1040.

46. Keller DI, Acharfi S, Delacrétaz E, et al. A novel mutation in SCN5A, delQKP 1507–1509, causing long QT syndrome: Role of Q1507 residue in sodium channel inactivation. *J Mol Cell Cardiol*. 2003;35:1513-1521.

47. Makiyama T, Akao M, Shizuta S, et al. A novel SCN5A gain-of-function mutation M1875T associated with familial atrial fibrillation. *J Am Coll Cardiol*. 2008;52:1326-1334.

48. Fertleman CR, Baker MD, Parker KA, et al. SCN9A Mutations in paroxysmal extreme pain disorder: Allelic variants underlie distinct channel defects and phenotypes. *Neuron*. 2006;52:767-774.

49. Huang J, Vanoye CG, Cutts A, et al. Sodium channel Na$_V$1.9 mutations associated with insensitivity to pain dampen neuronal excitability. *J Clin Invest*. 2017;127:2805-2814.

50. Wengert ER, Miralles RM, Wedgwood KCA, et al. Somatostatin-Positive interneurons contribute to seizures in SCN8A epileptic encephalopathy. *J Neurosci*. 2021;41:9257-9273.

51. Liu Y, Schubert J, Sonnenberg L, et al. Neuronal mechanisms of mutations in SCN8A causing epilepsy or intellectual disability. *Brain*. 2019;142:376-390.

52. Goldberg EM. Rational small molecule treatment for genetic epilepsies. *Neurotherapeutics*. 2021;18:1490-1499.

53. Simkin D, Kiskinis E. Modeling pediatric epilepsy through iPSC-based technologies. *Epilepsy Curr*. 2018;18:240-245.

54. Spratt PWE, Alexander RPD, Ben-Shalom R, et al. Paradoxical hyperexcitability from NaV1.2 sodium channel loss in neocortical pyramidal cells. *Cell Rep*. 2021;36:109483.

55. Zhang J, Chen X, Eaton M, et al. Severe deficiency of the voltage-gated sodium channel NaV1.2 elevates neuronal excitability in adult mice. *Cell Rep*. 2021;36:109495.

56. Que Z, Olivero-Acosta MI, Zhang J, et al. Hyperexcitability and pharmacological responsiveness of cortical neurons derived from human iPSCs carrying epilepsy-associated sodium channel nav1.2-L1342P genetic variant. *J Neurosci*. 2021;41:10194-10208.

57. van Hugte EJH, Lewerissa EI, Wu KM, et al. SCN1A-deficient excitatory neuronal networks display mutation-specific phenotypes. *Brain*. 2023;146(12):5153-5167.

58. Yao Z, van Velthoven CTJ, Nguyen TN, et al. A taxonomy of transcriptomic cell types across the isocortex and hippocampal formation. *Cell*. 2021;184:3222-3241.e26.

59. Tasic B, Menon V, Nguyen TN, et al. Adult mouse cortical cell taxonomy revealed by single cell transcriptomics. *Nat Neurosci*. 2016;19:335-346.

60. Tasic B, Yao Z, Graybuck LT, et al. Shared and distinct transcriptomic cell types across neocortical areas. *Nature*. 2018;563:72-78.

61. Hodge RD, Bakken TE, Miller JA, et al. Conserved cell types with divergent features in human versus mouse cortex. *Nature*. 2019;573:61-68.

62. Lin HC, He Z, Ebert S, et al. NGN2 Induces diverse neuron types from human pluripotency. *Stem Cell Reports*. 2021;16:2118-2127.

63. Bando Y, Irie K, Shimomura T, et al. Control of spontaneous Ca2+ transients is critical for neuronal maturation in the developing neocortex. *Cerebral Cortex*. 2016;26:106-117.

64. Vitali I, Fièvre S, Telley L, et al. Progenitor hyperpolarization regulates the sequential generation of neuronal subtypes in the developing neocortex. *Cell*. 2018;174:1264-1276.e15.

65. Lam RS, Töpfer FM, Wood PG, Busskamp V, Bamberg E. Functional maturation of human stem cell-derived neurons in long-term cultures. *PLoS One*. 2017;12:e0169506.

66. Lu C, Shi X, Allen A, et al. Overexpression of NEUROG2 and NEUROG1 in human embryonic stem cells produces a network of excitatory and inhibitory neurons. *FASEB J*. 2019;33: 5287-5299.

67. Schafer ST, Paquola ACM, Stern S, et al. Pathological priming causes developmental gene network heterochronicity in autistic subject-derived neurons. *Nat Neurosci*. 2019;22: 243-255.

68. Lancaster MA, Renner M, Martin CA, et al. Cerebral organoids model human brain development and microcephaly. *Nature*. 2013;501:373-379.

69. Bershteyn M, Nowakowski TJ, Pollen AA, et al. Human iPSC-derived cerebral organoids model cellular features of lissencephaly and reveal prolonged mitosis of outer radial Glia. *Cell Stem Cell*. 2017;20:435-449.e4.

70. Johnson MB, Sun X, Kodani A, et al. Aspm knockout ferret reveals an evolutionary mechanism governing cerebral cortical size. *Nature*. 2018;556:370-375.

71. Murayama AY, Kuwako KI, Okahara J, et al. The polymicrogyria-associated GPR56 promoter preferentially drives gene expression in developing GABAergic neurons in common marmosets. *Sci Rep*. 2020;10:21516.